Tuberculosis susceptibility in genetically diverse mice reveals functional diversity of neutrophils

Running title: Tuberculosis susceptibility in genetically diverse mice

Mariëtta M. Ravesloot-Chávez[1], Erik Van Dis[2], Douglas Fox[2], Xammy H. Nguyenla[2], Sagar L. Rawal[2], Mallory A. Ballinger[3], Henry Thomas[3], Dmitri Kotov[2], Russell Vance[2], Michael W. Nachman[3], Sarah A. Stanley[2,4]

1. Department of Plant and Microbial Biology, University of California Berkeley, California 94720, USA.
2. Division of Immunology and Pathogenesis, Department of Molecular and Cell Biology, University of California Berkeley, California 94720, USA.
3. Department of Integrative Biology, University of California Berkeley, California 94720, USA.
4. School of Public Health, Division of Infectious Disease and Vaccinology, University of California Berkeley, California 94720, USA

Summary. Infection of a new collection of wild-derived mice with *Mtb* reveals differences in the outcome of infection associated with unique immunological phenotypes.

Abstract

Tuberculosis (TB) is a heterogenous disease in humans with individuals exhibiting a wide range of susceptibility. This heterogeneity is not captured by standard laboratory mouse lines. We used a new collection of 19 wild-derived inbred mouse lines collected from diverse geographic sites to identify novel phenotypes during *Mycobacterium tuberculosis* (*Mtb*) infection. Wild-derived mice have heterogenous immune responses to infection that result in differential ability to control disease at an early timepoint. Correlation analysis with multiple parameters including sex, weight, and cellular immune responses in the lungs revealed that enhanced control of infection is associated with increased numbers of CD4 T cells, CD8 T cells and B cells. Surprisingly, we observed a negative correlation between IFN-γ production and control of infection. Although in most lines high neutrophils were associated with susceptibility, we identified a mouse line that harbors high neutrophils numbers yet controls infection. Using single-cell RNA sequencing, we identified a novel neutrophil signature associated with failure to control infection.

Introduction. *Mycobacterium tuberculosis* (*Mtb*) infection causes a wide range of disease outcomes in humans. Whereas most infected individuals never develop active disease and are able to control infection for their lifetimes, some individuals are highly susceptible to infection and develop active tuberculosis. Patients with active disease show heterogeneity in disease progression. Additionally, the timing of disease onset after initial infection and disease outcome varies from individual to individual (Cadena et al., 2017). This heterogeneity in human responses suggests that tuberculosis (TB) is a complex genetic disease. Surprisingly, there is only a limited understanding of the genetic factors that contribute to disease progression or control of infection. Indeed, GWAS studies have identified a small number of genetic factors that underlie the variability of responses to *Mtb* in humans including interferon-γ (*IFNG*), interferon-γ receptor (*IFNGR1*), interleukin-12 subunit p40 (*IL12B*) and interleukin-12 receptor b-1 chain (*IL12RB1*) (Qu et al., 2011). However, many questions remain regarding what factors determine susceptibility to infection. Despite the clear importance of IFN-γ for control of mycobacterial infection, new vaccine candidates that elicit IFN-γ producing T cells in human volunteers do not elicit complete protection from infection, suggesting that additional protective mechanisms that have yet to be identified may be essential (Tameris et al., 2013; Tait et al., 2019). Similarly, several immune signatures have been associated with active disease in tuberculosis patients, including type I IFN and neutrophils (Donovan et al., 2017). However, there has been little consensus on signatures that will predict the course of disease in patients, possibly in part due to the heterogeneity of mechanisms that lead to active disease (Nogueira et al., 2022).

The murine model of TB infection is a useful tool for analysis of host immune responses to infection due to the abundance of available reagents, ability to precisely control experimental conditions, and ease of genetic manipulation. Importantly, the mouse model captures much of what is known about human immune responses to *Mtb*, including the importance of CD4 T cells and IFN-γ for immune control of infection (Green et al., 2013; Caruso et al., 1999; Flynn et al., 1993; Scanga et al., 2000; Cooper et al., 1993). However, current mouse models fail to recapitulate several aspects of *Mtb* infection, including spontaneous resolution of infection as well as the widely varying susceptibility and patterns of disease seen in humans. Although there are minor differences in susceptibility to infection, most commonly used mouse lines all exhibit similar infection dynamics and characteristics. However, despite the limited diversity of common laboratory lines, comparison of divergent phenotypes followed by genetic mapping has identified loci that contribute to susceptibility to mycobacterial infection, leading to valuable insights into immune factors that influence susceptibility to infection. An example is the characterization of

the *Sst1* locus, which regulates type I IFN signaling through the gene *Sp140,* a repressor of type I IFN (Ji et al., 2019; Pan et al., 2005; Kramnik et al., 2000, 1998). Excessive production of type I IFN in *Sst1* susceptible (*Sst1*^{s}) mice, which have a loss of function mutation of *Sp140*, elicits increased IL-1 receptor antagonist (IL1-Ra) expression which competes with IL-1 for binding to the IL-1R. IL-1 is crucial for control of infection and the functional deficiency in IL-1 signaling in *Sst1*^{s} mice results in increased susceptibility to *Mtb* (Ji et al., 2019, 2021). Analysis of the phenotype of these highly susceptible mice led to the discovery of a mechanism by which type I IFN is detrimental to host infection. These studies suggest that increasing the genetic diversity in mouse models will lead to the discovery of additional genetic loci that are important for modulating the outcome of *Mtb* infection.

Historically, most *Mtb* studies in the mouse model have been conducted using only a handful of lines; C57BL/6 (B6), BALB/C and C3Heb/FeJ. In order to increase genetic diversity, new collections of mice have been established. The Collaborative Cross (CC) model was founded by crossing 5 common laboratory lines and 3 wild-derived lines (Churchill et al., 2004). Further breeding of the CC lines created the Diversity Outbred (DO) mouse collection, which is maintained as outbred population through random crossings. This is currently the most diverse mouse resource available (Svenson et al., 2012). Both cohorts have been used for the study of *Mtb* infection and display a range of disease phenotypes, including enhanced control or susceptibility to infection compared to standard laboratory lines (Smith et al., 2016; Niazi et al., 2015; Gopal et al., 2013). Infection of the DO cohort with *Mtb* revealed correlations between disease pathology and neutrophil influx, recapitulating features seen in human lung infections, in addition to identifying new inflammatory biomarkers that correlate with active human disease (Niazi et al., 2015; Koyuncu et al., 2021). Furthermore, these cohorts have been used to identify the genetic basis of disease responses. For example, the susceptibility of CC042 line is associated with the loss of *Itgal* expression, an integrin required for T cell trafficking to the lung, resulting in decreased T cell trafficking and IFN-γ production in the lungs of infected animals (Smith et al., 2019).

Studies using CC and DO mice demonstrate the power of genetically diverse mice for identifying novel host regulators of immunity to *Mtb* (Smith et al., 2022). However, it is unclear whether these collections capture the full spectrum of genetic diversity that exists in house mouse populations. To increase the genetic diversity of house mice available for the analysis of complex phenotypes, researchers recently created a set of 19 new inbred lines derived from

wild mice collected across different geographic regions (Phifer-Rixey et al., 2018; Moeller et al., 2018; Suzuki et al., 2020). Unlike CC and DO mice, these new lines are all from the *Mus musculus domesticus* subspecies of house mouse. The use of a single subspecies to establish this cohort is beneficial, as it limits allelic conflicts that can arise from crossing different subspecies. This allows for the maintenance of natural genetic heterogeneity and makes the presence of genomic "blind spots" – regions of the genome that are the same in all the lines – less likely (Salcedo et al., 2007; Yang et al., 2011). The mice that constitute this collection were originally collected across a latitudinal gradient from Brazil to Canada and show significant phenotypic diversity, including size, body mass index and lipid and glucose metabolism (Phifer-Rixey et al., 2018). Each line has been inbred through sib-sib mating for at least 10 generations, providing the benefit of the genetic reproducibility of laboratory derived lines.

This new collection of wild derived inbred lines represents a unique resource for identifying genetically diverse mice with enhanced or diminished susceptibility to *Mtb* infection and eventually, genes that control the host response to *Mtb* infection. Here we characterize 17 lines from this collection to identify lines that exhibit diminished control of *Mtb* infection at an early timepoint after infection (21 days) and analyze the accompanying immune responses. This is the first report of the use of this collection of mice for infectious disease or immunology-related phenotypes. Infection of the genetically diverse mouse lines reveals a range of responses with several lines showing higher susceptibility to *Mtb* compared with standard B6 mice. New susceptible lines of mice will be useful for identifying new mechanisms of susceptibility to infection. In addition, we have identified heterogeneity in immune responses to infection that are distinct from known mouse lines, including robust control of infection in the absence of a strong Th1 T cell response, and effective control of infection in the presence of elevated neutrophils. Our findings suggest that these mice will be useful not only for investigation of additional phenotypes in the context of TB infection but also may be useful for identifying novel immunological phenotypes more generally.

Results

Wild derived mouse lines display variability in immune responses and susceptibility to *M. tuberculosis* infection. The cohort of wild-derived mice used in this study was established using outbred mice originally collected from 5 different localities across the Americas: Edmonton (EDM), Alberta, Canada; Saratoga Springs (SAR), New York, United States of America; Gainesville (GAI), Florida, United States of America; Tucson (TUC), Arizona, United States of

America and Manaus (MAN), Amazonas, Brazil (Figure 1A). Multiple individuals were trapped at each locale, and used to create multiple, independent lines from an individual location. These mice exhibit a variety of phenotypic differences, including body weight, body length, body mass index (BMI) and glucose and lipid metabolism (Phifer-Rixey et al., 2018). Although there is within-group heterogeneity, separate lines of mice collected from a single location are in general more closely related genetically than mice collected from different locales (Ferris et al., 2021). We hypothesized that the genetic diversity of these mouse lines would contribute to heterogeneity in their capacity to control *Mtb* infection. We focused on a single timepoint, 21 days post infection, to specifically identify early loss of control. Observing enhanced control of infection is also possible, though less likely to be observed at this relatively early timepoint after the onset of adaptive immunity. Mice were challenged with aerosolized *Mtb* and the bacterial burden was assessed by colony-forming units (CFU) after 3 weeks of infection. CFU was normalized to inoculation dose day 1 post infection to correct for any variability in inhaled bacterial load between mouse lines with different activity levels, sex, or different days of infection. The median bacterial burden varied over 100-fold between mice from different locales (Figure 1B). Surprisingly, individual mouse lines that originated from the same locale demonstrated a wide variation in susceptibility, suggesting that genetic heterogeneity within the closely related lines can influence the outcome of infection. Bacterial burdens in the lungs of mice from the MANC line are significantly higher compared to the closely related MANA, MANB and MANE lines which are approximately as resistant as the standard B6 (Figure 1C). Mice from the MAND line show an intermediate phenotype. We also observed significant variability in bacterial burdens in mice from Saratoga Springs. Whereas SARA and SARC mice are at least as resistant to infection as the standard B6, SARB lines harbor significantly more bacteria in the lungs at 3 weeks post infection (Figure 1D). Smaller differences in susceptibility are found in the lines from Tucson, Gainesville, and Edmonton (Figure S1A-C).

A low BMI has been shown to be a risk factor for tuberculosis in humans (Lönnroth et al., 2010). Because the different lines of wild mice vary considerably in body weight even when provided the same diet, we examined whether differences in body weight could account for differences in the ability to control infection. For this analysis we focused on the Saratoga Springs and Manaus lines of mice where we observed the highest amount of variability in control of infection. We found that there were significant differences in the starting weight of mice prior to infection when comparing the different lines, with a trend towards increased body weight in mice from

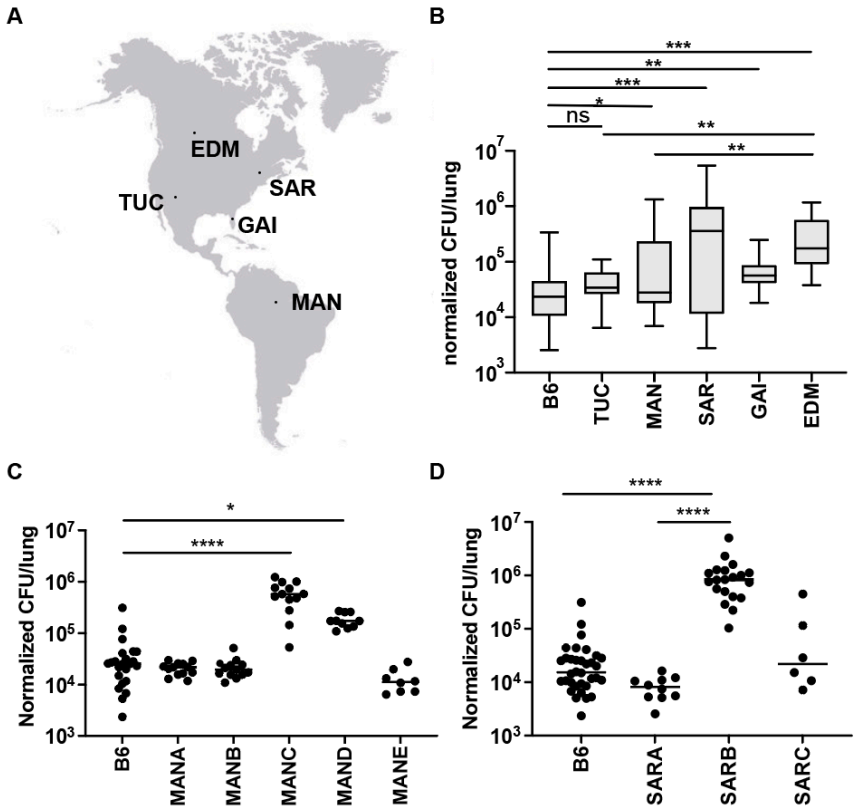

Figure 1. Mouse lines from different geographical regions show variable susceptibility to *Mtb* infection. (A) Mice were collected from five different sites across the Americas and inbred to generate individual genetic lines from each location. (B) Bacterial burden in the lungs of the mice derived from the different locations at 21 days post infection with aerosolized *Mtb*. Comparison of the susceptibility among genetically distinct Manaus lines (C) or Saratoga lines (D) infected with aerosolized *Mtb*. The average inoculum dose is 400 cfu/mouse. CFU data was normalized to CFU enumeration on day 1 to correct for variation in inoculum dose between experimental days. EDM: Edmonton, SAR: Saratoga Springs, TUC: Tucson, GAI: Gainesville, MAN: Manaus. Data represent 2-6 independent experiments for each mouse line with 6-34 mice per line. Each dot represents a mouse. The *p* values were determined using a Kruskal-Wallis ANOVA. *$p < 0.05$, **$p < 0.005$, ***$p < 0.0001$, ****$p < 0.0001$.

Saratoga Springs (Figure S1D). However, we did not find a correlation between body weight and TB control in these well-nourished mice (Figure S1E). Similarly, previous reports have suggested that sex plays a role in susceptibility to infection, with females being more susceptible to TB infection in both mice and humans. We also observed no differences in bacterial burden at 21 days post infection between male and female mice (Figure S1F). This is not surprising as demonstrated differences in the ability of male and female mice to control infection emerged only at late timepoints ~200 days after infection (Dibbern et al., 2017).

We next reasoned that genetically determined differences in immune responses to infection might underlie the differences in susceptibility observed between different lines of wild-derived mice. To identify immune correlates of bacterial burden in the lungs of the infected wild mouse lines we evaluated the presence of major immune cells thought to play a role in infection using flow cytometry in parallel with CFU counts at 21 days post infection. We observed variability in the relative proportions of macrophages, neutrophils, CD4 T cells, CD8 T cells and B cells when comparing individual lines (Figure 2A-E). The most striking differences observed were in CD11b+Ly6G+ neutrophils, both when comparing individual lines isolated from a single

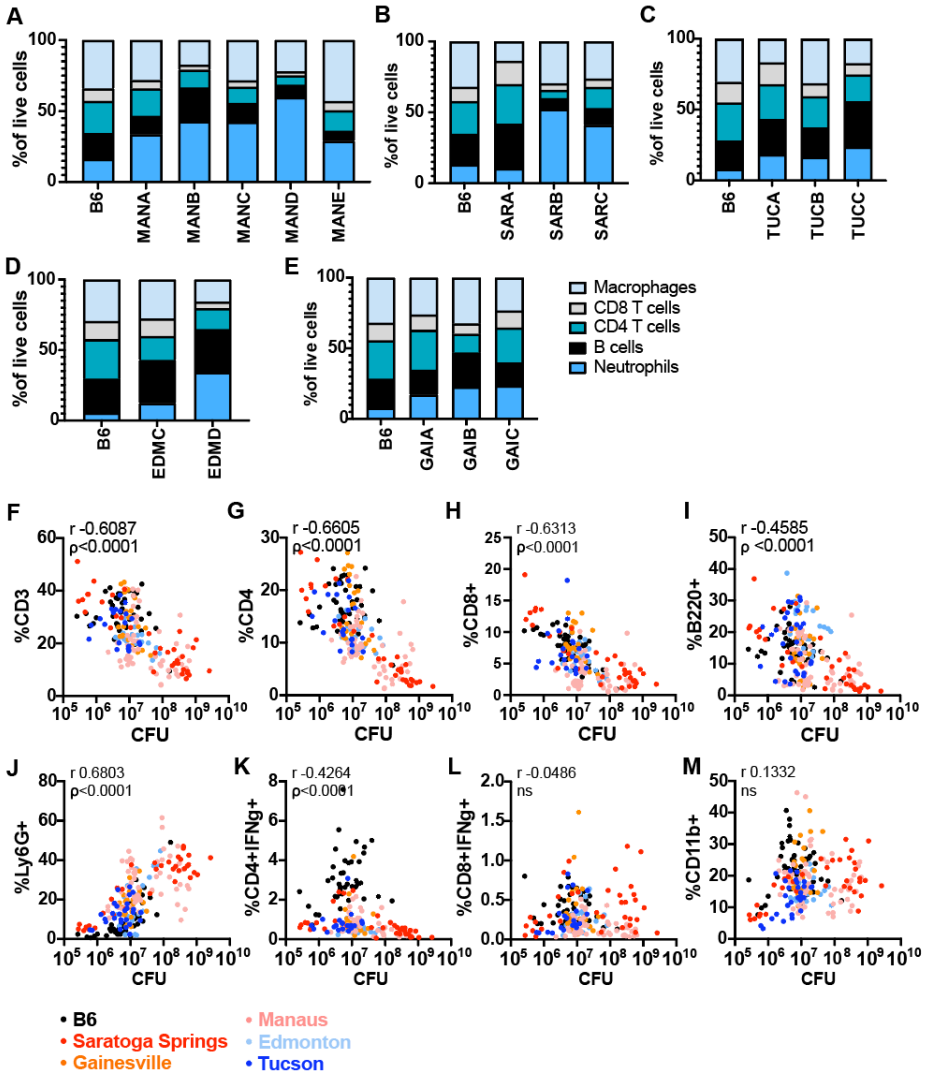

Figure 2. Genetic diversity translates into variability in bacterial burden and immune cells in the lung during *Mtb* infection. Cellular percentages were enumerated in the lungs using flow cytometry at 21 days post infection with *Mtb* between and within mouse lines from different locales (A-E). The correlation between immune cell type and CFU in the lung is depicted for individual mice (F-M). Data represent 2-6 independent experiments for each mouse line with 6-34 mice per line. The *p* value was determined using two-tailed Spearman correlations.

geographic site, and when comparing mice originally derived from different locales (Figure 2A-E).

In order to determine whether observed differences in the proportions of immune cells may drive the outcome of infection, we examined correlations between cell type and bacterial burden. We found significant correlations between the proportion of CD3+, CD4+, CD8+ and B220+ cells with control of infection, with larger proportions of these cells corresponding to lower CFU in the lung (Figure 2F-I). In contrast, we found that the proportion of neutrophils in the lung could explain approximately 60% of the variation seen in the wild-derived mice, with higher neutrophil burden associated with higher CFU in the lungs (Figure 2J). This is consistent with numerous studies of susceptible mice on the B6 background that have pointed to a role for excessive infiltration of neutrophil in promoting lung pathology and susceptibility to *Mtb* infection (Kimmey et al., 2015; Mishra et al., 2017; Nair et al., 2018; Dorhoi et al., 2010). Production of IFN-γ by T cells is known to be important for control of infection (Cadena et al., 2016; Mogues et al., 2001; Green et al., 2013; Bold and Ernst, 2012). As expected, B6 mice exhibit a high proportion of IFN-γ producing CD4 T cells and lower bacterial burden in the lungs compared to several wild mice lines (Figure 2K). This was particularly evident in mice from Saratoga Springs (SAR). The SARA line controls bacterial CFU in the lungs in the presence of very few IFN-γ producing CD4 T cells (Figure S2). No correlations were found between bacterial burden and the proportion IFN-γ producing CD8 T cells or CD11b+ cells (Figure 2L-M). The overall variation in bacterial burden and immune cells present in the lung among and between the locales indicates the heterogeneity in underlying immune responses to *Mtb* infection. The notable differences between the wild-derived mouse lines and B6 mice shows the potential for identifying novel mechanisms of susceptibility to infection in these mice.

Macrophages from Manaus lines show no intrinsic defects that correlate with control of infection. Despite being closely genetically related, the Manaus lines show distinct susceptibilities *to Mtb*. Whereas most of the tested lines control infection in the lungs as well as B6, the MANC line is significantly more susceptible to infection (Figure 1C). We therefore focused on these lines for a more in-depth immunological analysis. First, we tested whether impaired bacterial restriction in the MANC line can be explained by differences in cell intrinsic responses in host cells. Macrophages are central to *Mtb* infection, serving both as the host cell, the cell responsible for killing the bacteria, and an important source of cytokines that regulate infection (Cohen et al., 2018; Srivastava et al., 2014; Domingo-Gonzalez et al., 2016; Ravesloot-Chávez et al., 2021). To elucidate whether macrophage responses differ between

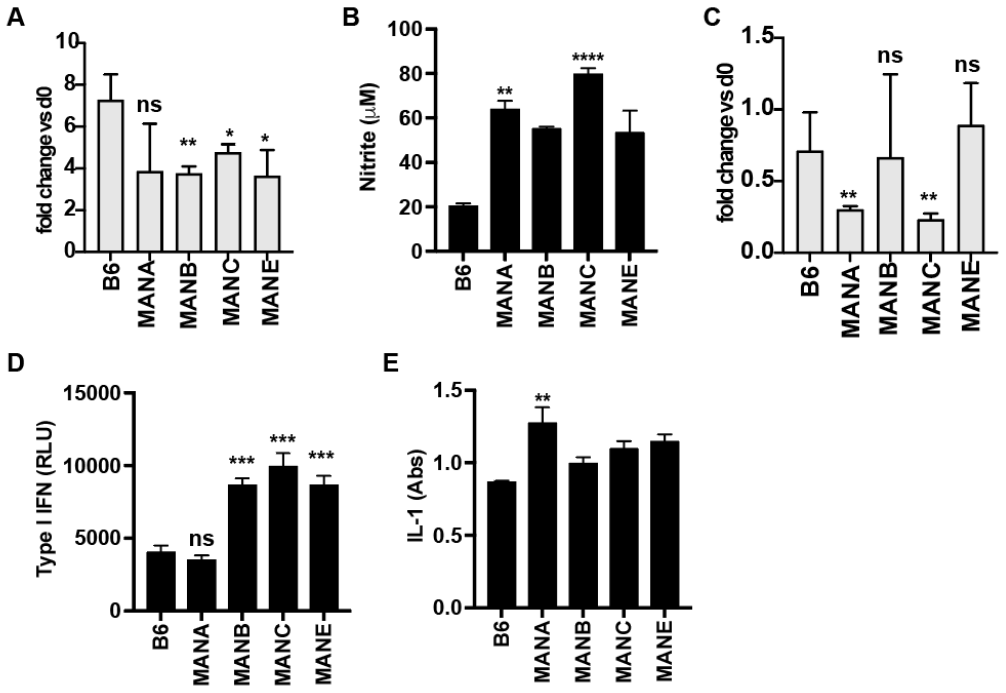

Figure 3. Intrinsic control of infection and response to IFN-γ is not impaired in macrophages from wild-derived mice. (A) BMDM isolated from indicated mouse lines were infected with *Mtb* and bacterial growth was determined at 4 days post infection by enumerating CFU. (B) The presence of nitrite in the supernatant was determined by Griess assay at 48 hours post infection. (C) IFN-γ activated BMDM were infected with *Mtb* and CFU were measured on day 4 post infection. Production of type I IFN (D) or IL-1 (E) was measured at 24 hours post infection with reporter cells lines. Data are a representative of 2 independent experiments. The *p* values were determined using a Kruskal-Wallis ANOVA. $^{**}p < 0.005$, $^{****}p < 0.0001$.

mouse lines, bone marrow-derived macrophages from four Manaus lines were prepared and infected with *Mtb* followed by quantification of bacterial burden and cytokine production. Macrophages from all the tested lines, including B6, allow the growth of *Mtb* in the absence of exogenous cytokine stimulation (Figure 3A), with none of the lines exhibiting a loss of control relative to B6. Indeed, we observed a slight decrease in bacterial replication in MANB, MANC and MANE relative to B6 (Figure 3A). Additionally, all macrophages responded similarly to IFN-γ stimulation, producing significantly more nitric oxide (NO) upon infection than is observed with B6 (Figure 3B). Similarly, we did not observe any defects in IFN-γ based control of infection at the macrophage level as all MAN lines controlled infection as well or better than the standard B6 (Figure 3C). Thus, differences in cell intrinsic control of infection do not obviously play a role in the susceptibility of the MANC line to *Mtb* infection.

Type I IFN is known to be a major driver of susceptibility in mice, and possibly humans (Ji et al., 2019; Dorhoi et al., 2014; Desvignes et al., 2012; Antonelli et al., 2010; Berry et al., 2010; Zak et al., 2016; Singhania et al., 2018; Scriba et al., 2017; Llibre et al., 2019). Macrophages from *Sp140*$^{-/-}$ mice that are highly susceptible to infection produce excessive type I IFN upon immune stimulation, recapitulating the high type I IFN/low IL-1 signaling phenotype of these animals *in vivo.* We next tested whether increased type I IFN or impaired IL-1 production by infected macrophages could underlie the high bacterial burden. Macrophages were infected with *Mtb* and levels of type I IFN were assessed at 24h post infection using interferon-stimulated response element (ISRE) L929 reporter cells (Jiang et al., 2005). We found that macrophages isolated from three MAN lines (MANC, MANB, MANE) produced significantly more type I IFN than B6 or MANA (Figure 3D), however these findings did not correlate with the ability to control infection *in vivo* (Figure 1C). We also measured IL-1 bioactivity in the supernatants of infected macrophages using the HEK-Blue IL-1R cell line and found that *in vitro* production of IL-1 was comparable to other Manaus genotypes and to B6. Taken together, none of the Manaus lines appear to have major macrophage intrinsic defects that would explain the observed differences in control of infection *in vivo.*

Heterogeneity in neutrophil phenotypes drives differences in bacterial burden.
Neutrophils possess potent antimicrobial mechanisms, yet their role in host defense during *Mtb* infection is not well defined. In human tuberculosis, neutrophils are generally associated with active disease and pathogenesis (Gopal et al., 2013; Eum et al., 2010; Lowe et al., 2012). The vast majority of mouse lines with excessive accumulation of neutrophils in the lung have high bacterial burdens in the lung and are susceptible to infection (Nandi and Behar, 2011; Mishra et al., 2017; Eruslanov et al., 2005; Niazi et al., 2015; Lyadova et al., 2010; Marzo et al., 2014; Keller et al., 2006). Interestingly, the majority of the Manaus lines show high neutrophilic influx to the lungs compared to B6 mice, despite the strong variability in bacterial burden (Figure 2A, 1C). In general, the proportion of neutrophils in the lung is a clear predictor of susceptibility to infection across all lines examined (Figure 2J, $r = 0.6803$). Indeed, we observed strong correlations in the proportion of neutrophils in the lungs with susceptibility to infection in B6 mice, which overall have robust control of infection (Figure S3A) as well as mice from Saratoga Springs, which encompass both susceptible and resistant lines (Figure S3B). However, when examining mice from Manaus, we found a significantly decreased correlation in the proportion of neutrophils in the lungs and the total CFU, in line with our initial observation that these mice tend to have higher neutrophils in the lungs than B6 despite variability in CFU (Figure S3C).

These data suggest that mice from Manaus may have phenotypic heterogeneity in neutrophil populations that results in diminished correlation between neutrophils and susceptibility to infection.

Recently studies have suggested that neutrophils are functionally heterogenous cells and can participate in the inflammatory response in both protective and deleterious roles. This prompted us to investigate the phenotypes of neutrophils in the Manaus lines during infection. We first sought to recapitulate our CFU and neutrophil data in experiments where we focus only on B6 and Manaus lines. Mice from Manaus controlled infection with *Mtb* as well as B6 mice, as measured by CFU in the lungs at 21 days post infection, with the exception of the MANC line (Figure 4A). All Manaus mice have a higher proportion of neutrophils in the lungs (Figure 4B). In addition, when comparing the absolute number of neutrophils in the lungs of infected mice, MANB and MANC had elevated, roughly equivalent, absolute numbers of neutrophils in the lungs (Figure 4C), despite very different bacterial burdens (Figure 4A). We next tested whether the high neutrophilic influx in the lungs of MANC mice drives susceptibility to infection. We treated mice with an antibody targeting Ly-6G to deplete neutrophils. Antibody depletion resulted in a dramatic drop in CFU in the lungs of MANC mice (Figure 4D, E). Thus, in MANC mice, neutrophils are an important driver of susceptibility.

In order to elucidate the phenotypic differences of the cell populations in the different wild-derived mouse lines from Manaus, we used single-cell RNAseq (scRNAseq) to identify transcriptional changes in immune cells isolated from lungs of *Mtb* infected B6, MANA, MANB, and MANC mice at 21 days post infection. Using signature transcription factor, cytokine, and cell surface marker expression, the dataset was analyzed in the Seurat environment and major immune cell types in the lung were defined. Overall, transcriptional profiles indicated that the cell type composition was relatively similar across genotypes. The exception was an increase in cells identified as neutrophils (*Ly6G+, S100a8+*) in both MANB and MANC mice relative to the other genotypes, consistent with our flow cytometry data (Figure S3D-S3G).

To identify phenotypic heterogeneity within neutrophils, we subset neutrophils from all genotypes, identified variable features and rescaled the data within the subset, performed PCA dimension reduction and clustering and visualized the results with the UMAP reduction. Neutrophils clustered into 2 major populations (Figure 4F) and at least 9 well defined subpopulations (Figure 4G). B6, MANA and MANB neutrophils clustered together while MANC neutrophils remained quite distinct. MANB neutrophils exhibited some transcriptional

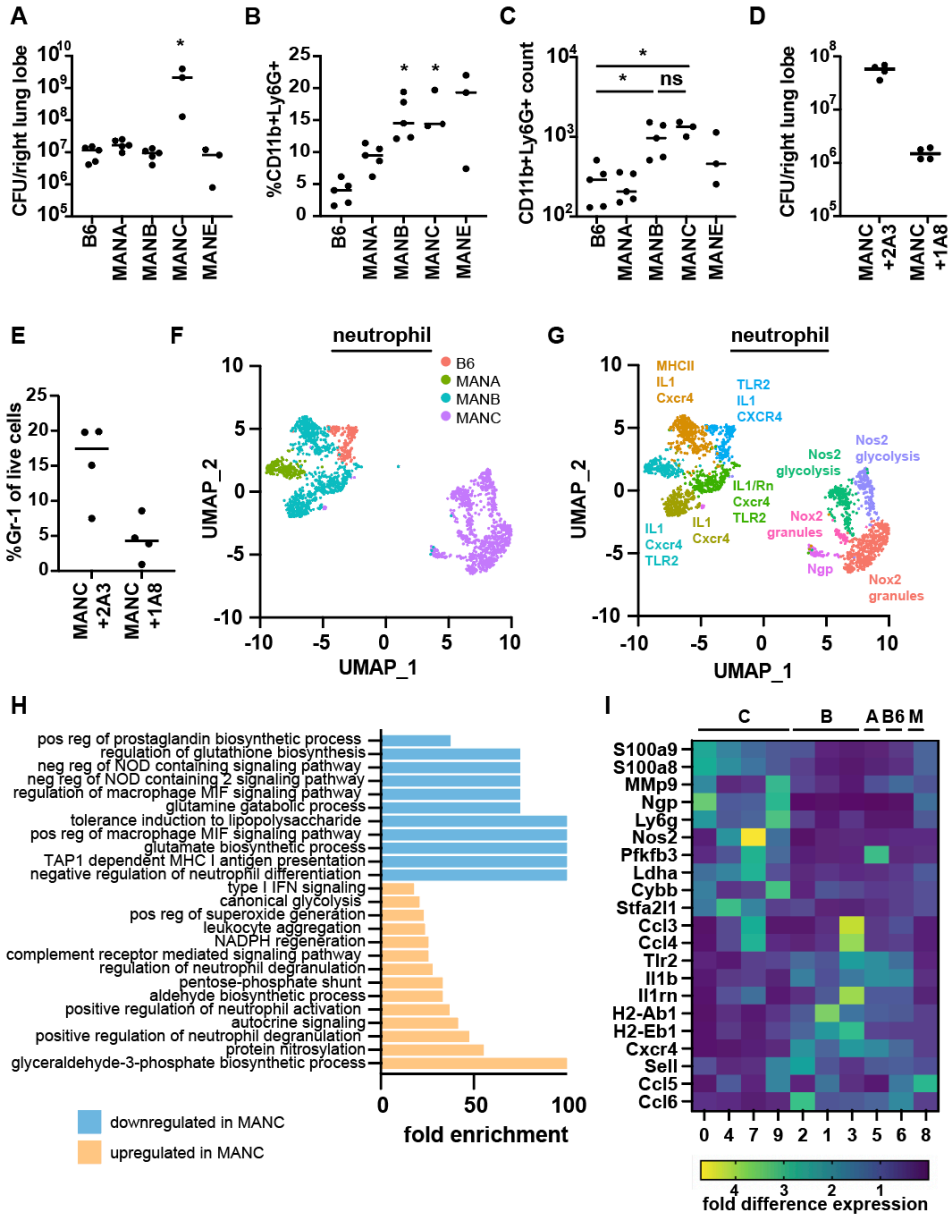

Figure 4. Diverse populations of neutrophils are present during infection of Manaus mice. (A) Bacterial burden in the in the lung was assessed in Manaus mice at 25 days post infection. (B-C) Percentages and absolute counts of CD11b+Ly6G+ cells in the lungs at 25 days post infection were enumerated by flow cytometry. (D-E) MANC mice were treated with neutrophil depleting antibody (1A8) or isotype control (2A3) every other day starting on day 11 post *Mtb* infection. Bacterial burden and neutrophil numbers were quantified on day 25 post infection. (F-G) UMAP clustering of neutrophils from scRNAseq data of live cells in the lung at 21 days post *Mtb* infection. Signature functional genes that are characteristic of each cluster are provided with color coding according to cluster. (H) Gene ontology enrichment analysis of pathways down or upregulated in MANC neutrophils compared with other neutrophil genotypes shows enrichment of genes involved in neutrophil activation and metabolism. (I) Comparison of gene expression between highly expressed genes in the MANC neutrophil clusters with expression in MANB (B), MANA (A), B6 and clusters of mixed genotype (M). CFU and antibody depletion data are a representative of 3 independent experiments. The *p* values were determined using Mann-Whitney U test (A) and Kruskal-Wallis ANOVA (B,C), $p < 0.05$. scRNAseq data represent a single experiment with tissues from 4 mice.

heterogeneity with two distinct neutrophil subpopulations distributed across two clusters (Figure 4F). B6 and MANA neutrophils were more homogeneous (Figure 4F). MANC clustered separately from neutrophils of any of the other genotypes and exhibited the most within genotype heterogeneity in neutrophil subsets (Figure 4G, 4F). MANB and MANC mice exhibit comparably elevated numbers of neutrophils in their lungs during *Mtb* infection despite a 2 log difference in bacterial burden (Figure 4A-C). We next sought to further characterize transcriptional differences in MANC neutrophils relative to other genotypes across all neutrophil subtypes. Aggregated together, neutrophils from MANC mice were enriched for GO biological processes indicative of neutrophil activation, including positive regulation of neutrophil activation, neutrophil degranulation, superoxide generation, and glycolysis (Figure 4H). GO processes downregulated in MANC neutrophils relative to B6 included antigen processing, prostaglandin biosynthesis, and NOD signaling (Figure 4H). These data suggest that neutrophils from MANC mice are more activated, and more likely to be engaging in processes that result in destruction of host tissue. Neutrophils from MANC mice express higher levels of neutrophil signature genes, including *S100a8/9, Ngp, and Ly6G* (Figure 4I). These neutrophils also express higher levels of genes associated with pathogen clearing and host tissue damage including inducible nitric oxide synthase (*Nos2),* NADPH oxidase (*Cybb*), and *Mmp9.* MANC neutrophils glycolytic signature includes higher expression levels of *Ldha* and *Pfkfb3.* MANC neutrophils clustered into subsets that were distinguished by differential expression of these marker genes (Figure 4G). In contrast, neutrophils from MANA, MANB, and B6 mice expressed higher levels of specific immune related genes relevant to defense against *Mtb* infection including *Tlr2, Il1b,* and MHC II isoforms *(H2-Ab1, H2-Eb).* Other genes that were highly differentially expressed between the lines were the chemokines *Ccl3, Ccl,4 Ccl5 Ccl6* (Figure 4I). Neutrophils from all lines expressed very low levels of immunosuppressive proteins and cytokines, with the exception of IL-1R antagonist (*Il1rn*) which was highly expressed by a subset of MANB neutrophils (Figure 4I). In summary, neutrophils in susceptible MANC mice exhibit a transcriptional program that is unique when compared with other MAN lines or to B6 mice.

Granuloma like structures in MANC mice are dominated by neutrophils and have a paucity of both macrophages and T cells. We used immunofluorescence microscopy to characterize granuloma like structures in MANB and MANC mice infected with *Mtb*. Both MANB and MANC lesions contained large numbers of neutrophils as determined by staining with both CD11b and Ly6G antibody (Figure 5A-D). Whereas neutrophils appeared as discrete cells within lesions of MANB mice (Figure 5A,B), neutrophils in MANC lesions appeared to form large

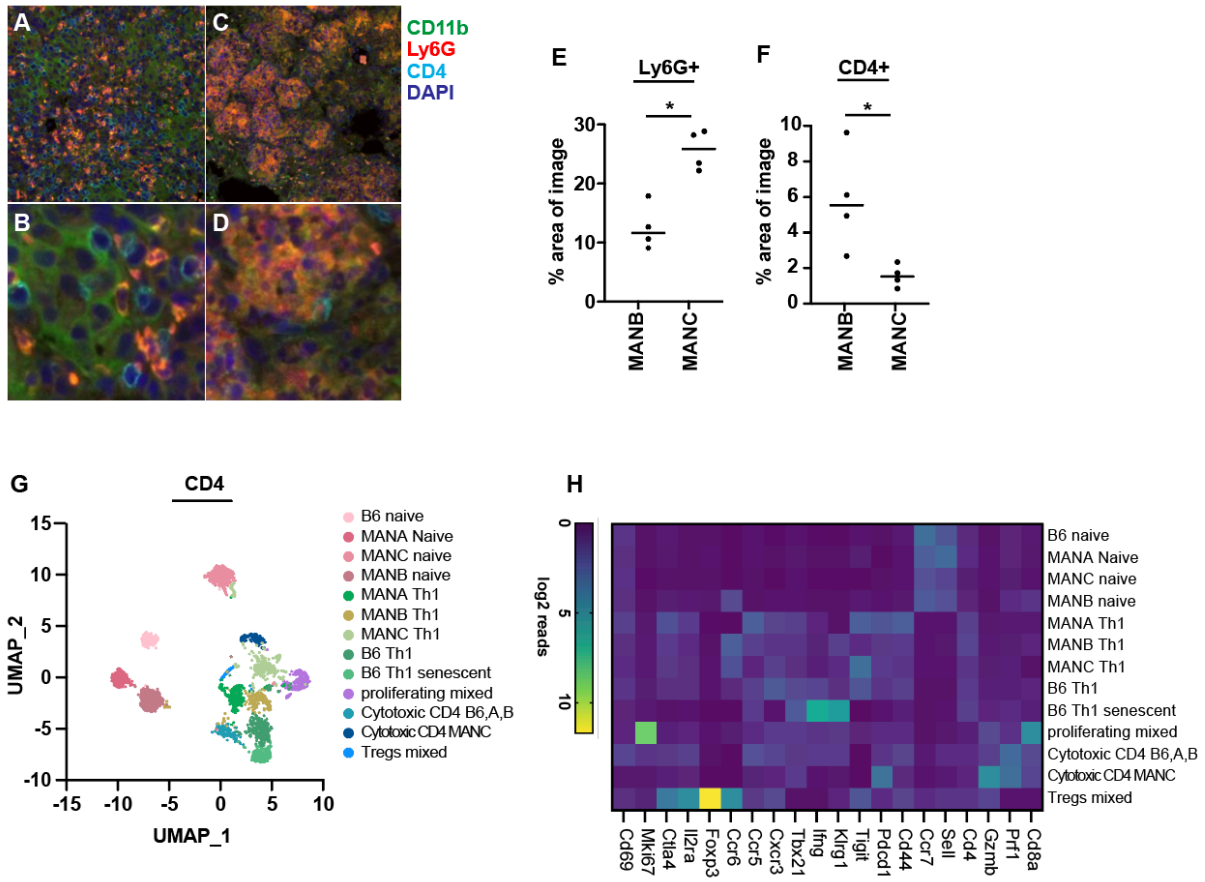

Figure 5. The cellular infiltrate in MANC lesions consists mainly of neutrophils.
(A-D) Immunofluorescent microscopy on fixed lung tissues from MANB (A, B) and MANC (C, D) mice at 21 days post infection. Surface area quantification of Ly6G+ (E) or CD4+ (F) staining in lung sections. (G) UMAP analysis of CD4 T cell subsets in the lung from scRNAseq expression data of Manaus and B6 mice. (H) Heatmap of scRNAseq expression data of T cell clusters from individual Manaus lines and clusters from mixed mouse lines. Significance calculation is students t-test, $p < 0.05$.

aggregates of cells (Figure 5C,D). In addition, there was twice the amount of neutrophil staining per area in MANC lesions relative to MANB (Figure 5E) and far fewer CD4 T cells within MANC lesions than within MANB lesions (Figure 5F). These data suggest that macrophages in lesions from MANC mice may differentially recruit neutrophils versus T cells, and/or that T cells may have an intrinsic defect in homing to lesions in MANC mice. To identify transcriptional differences in CD4 T cells and macrophage/monocyte populations that distinguish the lines of mice, we turned to our scRNAseq data. After subsetting CD4 T cells from all genotypes, renormalizing gene counts, PCA dimension reduction clustering and visualizing a UMAP reduction, we identified 13 clusters that correspond to clearly distinct CD4 differentiation states (Figure 5G). All genotypes possessed naïve CD4 T cells, Th1 differentiated T cells, Ki67+

proliferating T cells, and cytotoxic T cells expressing granzyme B and perforin (Figure 5G). B6 mice uniquely had a population of what appear to be terminally differentiated Th1 T cells that express KLRG1 and high levels of IFN-γ (Figure 5G). These cells have been previously identified as a non-protective T cell subset in B6 mice (Sakai et al., 2014; Cyktor et al., 2013; Lindenstrøm et al., 2013). It is interesting that none of the Manaus lines appear to have this subset of T cells, even in the susceptible MANC line. Other markers of T cell activation and differentiation including *Cd44, Pdcd1, Tigit,* and *Cd69* were not substantially different across mouse lines (Figure 5H), suggesting that major phenotypic differences in CD4 T cells themselves, separate from their propensity for trafficking into or surviving within the granuloma, do not underlie the susceptibility of MANC mice. We also did not observe major differences in chemokine or chemokine receptor expression of genes known to be required for T cell trafficking into the lung parenchyma (not shown). Signals required for T cell trafficking into lesions are unknown.

CD11b+/Ly6G- macrophage/monocyte like cells were also mapped using our scRNAseq data, and were found to fall into 14 distinct clusters, many but not all of which were genotype specific (Figure 6A, 6B). No clear pattern in terms of distribution of cell types emerged from analysis of markers for macrophages (*Adgre1),* monocytes (*Cx3cr1*), and inflammatory monocytes (*Ly6c*) (Figure 6C). However, similar to what we previously observed in neutrophils, monocyte/macrophages from MANC mice had a higher propensity to express *Nos2* (Figure 6C). No other genes indicative of macrophage function including *IL1b, Arg1, Tnf, and Cybb* were differentially expressed across genotypes (Figure 6C). Interestingly, MANC macrophages also exhibited very high levels of expression of *S100a9* and *S100a8*, genes more typically associated with neutrophil function (Figure 6C).

Global transcriptional changes in MANC immune cells reveal expanded expression of neutrophil markers across multiple cell lineages. Both macrophages and neutrophils from MANC mice express higher levels of *S100a8* and *S100a9* than cells from other genotypes. To identify differentially expressed genes in MANC mice whose expression patterns are preserved across multiple cell types, we analyzed scRNAseq data. Interestingly, we found that expression of a small number of genes was dramatically increased in MANC mice, and that this signature was dominated by genes that are often thought to be relatively neutrophil specific, including *Ngp* (neutrophil granule protein), *S100a9, S100a8* and *lcn2* (lipocalin 2) (Figure 6D). Higher expression of these genes was not solely driven by higher expression levels in neutrophils, as

we observed increased expression of these genes across all cell types analyzed, which included major immune cell populations as well as endothelial cells and fibroblast isolated from lungs (Figure 6E and not shown). To determine whether expression of highly neutrophil specific proteins has been observed in other cell types, we examined expression of *Ngp* across cell types in the ImmGen database (Heng et al., 2008) which hold curated expression data defined by immunological cell type and state. As expected, we found that expression of *Ngp* was observed at highest levels in neutrophils, with dramatically lower levels of expression across other immune cell types (Figure S4). Thus, expression of these neutrophil specific genes across many cell types appears to be a unique feature of MANC mice.

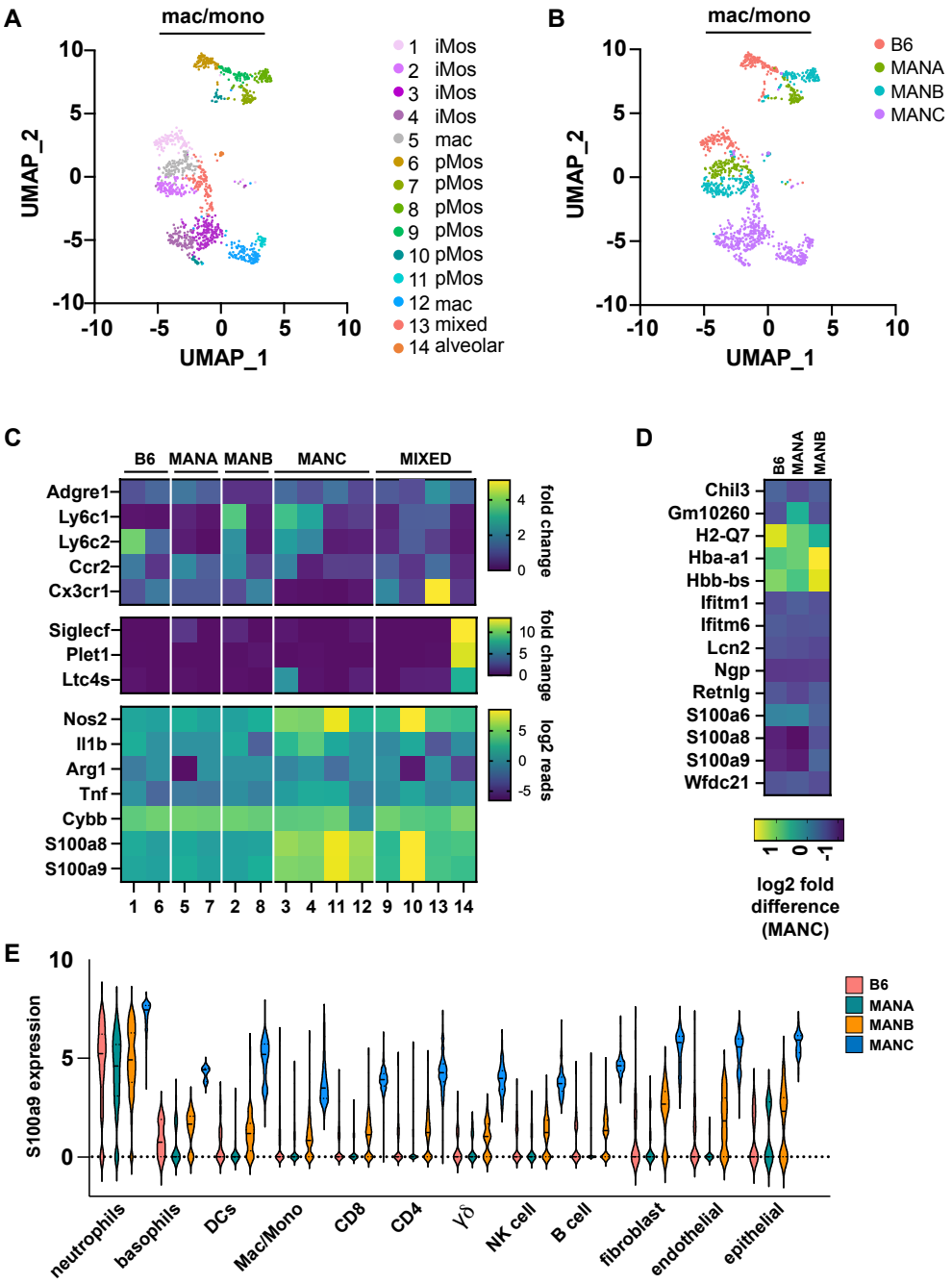

Figure 6. Expression of neutrophil markers across multiple cell lineages in MANC mice. (A) Unsupervised clustering of CD11b+Ly6G- monocyte/macrophage-like cells in the lung based on scRNAseq gene expression color coded by cluster (A) or genotype (B). (C) heat map of gene expression of markers of macrophage/monocyte subsets according to cluster and genotype. (D) Expression of indicated genes across all cell types comparing the B6, MANB, and MANC genotypes. (E) Violin plot of *S100a9* expression according to cell type and genotype. Inflammatory monocytes (iMos); patrolling monocytes (pMos).

Discussion

Developing immune based diagnostics and new vaccines for tuberculosis has been challenging, likely due in part to the heterogeneity of human responses to disease. Host and bacterial genetics and environmental factors combine to shape the variety of disease outcomes seen in human tuberculosis. Furthermore, studies of human immune responses are by their nature rarely able to distinguish mechanisms that are causative of, rather than merely correlative with, disease outcomes. Thus, it has been difficult to answer some of the most important questions in the field. First, we lack an understanding of why some individuals experience a failure of immunity that results in progression to active disease. Further, reliable biomarkers of successful control of tuberculosis remain elusive, despite the importance of such biomarkers for guiding the development of new and effective vaccines. The strength of animal models comes from the ability to deeply interrogate novel immunological phenotypes and uncover unrecognized mechanisms of infection control or susceptibility. Furthermore, the animal model can be used to establish causation based upon observations in humans. For example, there has been significant synergy between mouse and human immune studies for the establishment of type I IFN as an important driver of susceptibility to disease (Stanley et al., 2007; Moreira-Teixeira et al., 2020b; a; Berry et al., 2010). Identifying new immunological mechanisms in mice could lead to human studies focused on these mechanisms. Here we used a new collection of inbred wild mice to study the outcome of infection with *Mtb.* Wild mice exhibited a range in susceptibility at an early timepoint after infection as well as diversity in the immune responses to infection (Figure 1, 2). Our initial survey of these mice has identified several lines with interesting and novel phenotypes worthy of in-depth investigation including a unique neutrophil signature associated with susceptibility.

Neutrophils are thought to be an important driver of susceptibility to the outcome of tuberculosis in both mice and humans (Berry et al., 2010; Nandi and Behar, 2011; Mishra et al., 2017). It has been proposed that the neutrophils are detrimental to infection due to generation of lung inflammation and NETosis (Moreira-Teixeira et al., 2020a). It is still unclear what drives excess accumulation of neutrophils under different conditions. Further, neutrophils can adopt numerous phenotypes, and it is unclear whether all neutrophils are equally destructive during infection or whether specific neutrophil signatures are predictive of disease. Studying the role of neutrophils during *Mtb* infection has been challenging, due to the short lifespan and the subsequent difficulties of culturing neutrophils *ex vivo*. In addition, there are relatively few models of susceptibility to infection available for analysis. We found that neutrophils are highly abundant in

the lungs of infected MANC mice, and that neutrophils drive the susceptibility of this line (Figure 4A-E). This finding accords with what has been shown by previous studies of other highly susceptible mice (Kimmey et al., 2015; Mishra et al., 2017; Nair et al., 2018; Dorhoi et al., 2010). However, MANB mice also harbor elevated levels of neutrophils, yet control infection as well as the standard B6 control. Histological data from the lungs of MANC mice show Ly6G staining for neutrophils reveals large aggregates of staining within the lesions of MANC mice, whereas neutrophils in MANB mice are more discrete and dispersed throughout the tissue (Figure 5). scRNAseq expression analysis shows that neutrophil clusters from MANC mice have a high expression of genes that contribute to neutrophil degranulation as well as superoxide and nitric oxide production, indicating potential for tissue destruction during infection. In addition, neutrophils from these mice exhibit a more activated glycolytic transcriptional signature when compared with B6 or other MAN lines. The transcriptional phenotype of protected MANB mice is strikingly different from MANC, with an expression profile that is associated with protective genes, including *Tlr2* and *Il1b*. Whether these divergent phenotypes reflect differences in inherent immunological responses, or are driven by underlying differences in the capacity of these mice to control infection, will be an important topic for future study.

Another intriguing aspect of the immune response to *Mtb* is the role of IFN-γ during infection. IFN-γ is mainly produced by CD4 T cells early during infection and a lack of IFN-γ results in extreme susceptibility with mice succumbing to infection (Green et al., 2013; Flynn et al., 1993). Furthermore, IFN-γ is required for prevention of bacterial dissemination to other tissues (Sakai et al., 2016). However, increased IFN-γ responses in the lung do not seem to correlate with resistance to infection or improved responses to vaccination and can lead to exacerbated disease (Sakai et al., 2016; Leal et al., 2001; Majlessi et al., 2006; Mittrücker et al., 2007; Tameris et al., 2013). While local IFN-γ production might be necessary for full control of infection in B6 mice, additional research has shown effects of T cell mediated IFN-γ independent mechanisms that contribute to control of infection, including through GM-CSF production by CD4 T cells (Rothchild et al., 2014, 2017; Van Dis et al., 2022) and the production of IL-17 (Gallegos et al., 2011). Several mouse lines in the cohort showed restriction of bacterial growth in the first weeks post infection equally well but with widely differing IFN-γ+ T cell profiles. SARA mice exhibited enhanced control of bacterial burden (Figure 1D), but very low numbers of IFN-γ+ T cells compared to B6 mice (Figure 2K, S2). This suggests either optimal localization of the few IFN-γ producing T cells to the bacterial-containing lesions thereby allowing for highly efficient induction of local IFN-γ driven protective responses in the lesions, or

the presence of IFN-γ or T cell -independent control of infection. Further research is needed to determine the spatial interactions between T cells and other immune cells present in the lesions, including bacilli-containing macrophages. It has previously been shown that homing of *Mtb*-specific T cells to the lung parenchyma is essential for interaction with activated macrophages to induce control of infection, however signals that allow for T cell penetration into granulomas have not been fully elicited (Sakai et al., 2016). Finally, longitudinal studies are needed to determine whether control of infection in SARA mice persists over longer time periods.

The results presented here should inspire more in-depth mechanistic analysis of phenotypes observed in wild mouse lines by our group as well as others in the field. Ultimately, it will be important to identify genetic differences that underlie the differences in capacity to control disease. Intercrossing of these closely related lines may elucidate genetic loci that are responsible for underlying phenotypes, possibly due to the presence of genetic variants that are absent in standard mouse lines. This strategy has been used with success by the breeding of susceptible C3H and resistant B6 mice to identify the super susceptibility locus 1 (*Sst1*) (Kramnik et al., 2000) as well as through the study of genetically diverse cohorts including the collaborative cross and diversity outbred mice which resulted in the identification of susceptibility markers (Smith et al., 2019; Niazi et al., 2015).

In addition to the abovementioned phenotypes, many other interesting correlates of immunity were identified in these mice that are worthy of future investigation. For example, we found a correlation between higher B cell numbers and improved resistance to infection; whether B cells may play a role in infection control is a question that can be examined using these lines. These and other phenotypes may be important not only for tuberculosis, but for other studies of host immunity. We suggest that these wild mice will be a rich source of phenotype discovery for numerous fields, adding to the heterogeneity of models available for the study of disease.

Acknowledgments

We want to thank the members of the Stanley, Cox and Vance labs for helpful discussions. We thank Justin Y. Choi at the Functional Genomics Laboratory (UC Berkeley) for scRNAseq library preparation and sequencing, QB3 Genomics and the Vincent J. Coates Genomics Sequencing Laboratory (UC Berkeley) for scRNAseq sample sequencing, Qian Chen at the Center for Genomic Pathology Laboratory (UC Davis) for tissue embedding and sectioning and Wei Yang at NanoString Technologies for immunofluorescent microscopy staining. This work was supported by NIH R21AI146810 and NIH P01 AI063302 to SAS and by NIH RO1 GM074245 and NIH R01 GM127468 to MWN as well as a NSF Graduate Research Fellowship to MMR-C.

Materials and methods

Ethics statement

All procedures involving the use of mice were approved by the University of California (UC), Berkeley, Institutional Animal Care and Use Committee (AUP-2015-09-7979-2). All protocols conform to federal regulations and the National Research Council's *Guide for the Care and Use of Laboratory Animals*.

Mice

Wild-derived mouse lines from the Manaus (MANA, MANB, MANC, MANE), Saratoga Springs (SARA, SARB, SARC), Edmonton (EDMA, EDMC, EDMD), Tucson (TUCA, TUCB, TACC) and Gainesville (GAIA, GAIB, GAIC) locations were obtained from the Nachman laboratory (UC, Berkeley). Several lines from these cohorts have since been deposited to The Jackson Laboratory (Bar Harbor, ME) as a public resource (ManA/NachJ #035354; ManB/NachJ #035355; ManE/NachJ #035365; SarA/NachJ #035346; SarB/NachJ #035347; SarC/NachJ #035348; TUCA/NachJ #035358; TUCB/NachJ #035359; GaiC/NachJ #035352). C57BL/6J (#000664) mice were obtained from The Jackson Laboratory and bred in-house. For mouse weight measurements, male mice were housed singly in a cage to avoid social dominance effects on weights. Female mice were group housed and body weights were measured at 7 weeks old and prior to infection with *Mtb*.

Bacterial culture

Low passage stocks of *Mtb* Erdman were grown in Middlebrook 7H9 liquid medium supplemented with 10% albumin-dextrose-saline or on solid 7H10 agar plates supplemented with 10% Middlebrook oleic acid, albumin, dextrose, and catalase (BD Biosciences) and 0.4% glycerol. Frozen stocks of *Mtb* were made from liquid cultures and used for all *in vivo* infection experiments.

***In vivo* infections.** Mice were infected via the aerosol route with *Mtb* strain Erdman. Aerosol infection was done using a nebulizer and full-body inhalation exposure system (Glas-Col, Terre Haute, IN). Bacterial culture diluted in sterile water was loaded into the nebulizer calibrated to deliver ~400 bacteria per mouse, as measured by CFU in the lungs 1 day following infection (data not shown). Neutrophil depletion experiments were performed as described in Nandi and Behar (Nandi and Behar, 2011) using the anti-Ly6G monoclonal Ab (clone 1A8; BioXCell) or

isotype control (clone 2A3, BioXCell). Two hundred micrograms of Ab were injected every other day starting at day 11 post infection. Mice were sacrificed at 21 or 25 days post infection to measure CFU and immune responses in the lungs. For bacterial enumeration, the largest lung lobe was homogenized in PBS supplemented with 0.05% Tween 80, and serial dilutions were plated on 7H10 plates. CFU were counted 21 days after plating. The three smallest lung lobes were harvested into complete RPMI (supplemented with 10% fetal bovine serum, 2 mM L-glutamine, 100 U/mL penicillin/streptomycin, 1 mM sodium pyruvate, 20 mM HEPES, 55 μM 2-mercaptoethanol), and strained through a 40-μm Falcon strainer. Cells were washed, stained with antibodies used for cytokine and surface marker staining: live/dead (L34970; Thermo Fisher Scientific), CD4, CD3, CD8a, CD11b, B220, Ly-6G (100509, 100219, 100707, 101237, 103233, 127627, respectively; BioLegend) and fixed/permeabilized with BD Cytofix/Cytoperm Fixation/Permeabilization Solution Kit (554714; Thermo Fisher Scientific) before staining with antibody specific for IFN-γ (505816; BioLegend). Data were collected using a BD LSR Fortessa flow cytometer and analyzed using FlowJo Software (Tree Star, Ashland, OR).

IL-1 bioactivity reporter assay. The second largest lung lobe from infected mice was harvested into complete RPMI supplemented with Pierce proteinase inhibitor EDTA-free (Thermo Fisher Scientific), dissociated, and strained through a 40 μM Falcon strainer. Cells and debris were removed by a low-speed centrifugation (300g) followed by a high-speed centrifugation (2,000g) and stored at -80°C. Samples were assayed using HEK-Blue IL-1R cells (InvivoGen, San Diego, CA). A total of 3.75×10^4 cells per well were plated in 96-well plates and allowed to adhere overnight in DMEM supplemented with 10% FBS, 2 mM L-glutamine. Reporter cells were treated overnight with 100 μL of sample (consisting of 50 μL of cell-free lung homogenates and 50 μL of media), or recombinant mouse IL-1β (R&D systems 401-ML-005). Assays were developed using QUANTI-Blue (InvivoGen) according to the manufacturer's protocols and measured using a SpectraMax M2 microplate reader (Molecular Devices, San Jose, CA).

IFN-β bioactivity reporter assay. Interferon responsive ISRE-L929 cells were cultured in ISRE media (DMEM, 2 mM glutamine, 1 mM pyruvate, 10% heat inactivated FBS, and penicillin-streptomycin). Presence of type I interferon was assessed using lung homogenate as described above. Homogenates were applied in various dilutions to the interferon responsive ISRE-L929 cells (5×10^4 cells/well) in white, 96-well, tissue culture treated plates (Thermo Scientific Nunc). Cells were incubated for 4 hours, media aspirated, and cells were lysed with 30 μL Luciferase

cell culture lysis reagent (Promega Madison, WI). Finally, 100 µL of luciferase substrate solution (Promega) was added to each well and luminescence was measured using a Spectramax L luminometer (Molecular Devices).

qRT-PCR. The second largest lung lobe from infected mice was harvested into 500 µL RNAlater solution (Invitrogen Life Technologies, Carlsbad, CA) and stored at -80°C for qRT-PCR analysis. Tissues were transferred to 500 µL TRIzol (Invitrogen Life Technologies) and homogenized. Total RNA was extracted using chloroform, and the aqueous layer was further purified using RNeasy spin columns (Qiagen, Hilden, Germany). For qPCR, cDNA was generated from 1 mg RNA using Superscript III (Invitrogen Life Technologies) and oligo(dT) primers. Select genes were analyzed using Power SYBR Green qPCR master mix (Thermo Scientific). Each sample was analyzed in triplicate on a CFX96 real-time PCR detection system (Bio-Rad, Hercules, CA). CQ values were normalized to values obtained for GAPDH, and relative changes in gene expression were calculated as $\Delta\Delta C_Q$.

***In vitro* infections.** Bone-marrow was obtained from B6 and wild-derived mice and cultured in DMEM with 10% FBS, 2 mM L-glutamine, and 10% supernatant from 3T3–M-CSF cells for 6 days with feeding on day 3 to generate bone marrow-derived macrophages (BMDM). BMDM were plated into 96-well or 24-well plates with 5×10^4 and 3×10^5 macrophages/well, respectively, and were allowed to adhere and rest for 24 h. BMDM were then treated with vehicle or recombinant mouse IFN-γ at 6.25 ng/ml (485-MI, R&D Systems) overnight and infected with *Mtb* Erdman strain at a multiplicity of infection of 5 in DMEM supplemented with 5% horse serum and 5% FBS, unless otherwise noted. After a 4 h phagocytosis period, media was replaced with DMEM supplemented with 10% FBS, 2 mM glutamine and 10% M-CSF. For IFN-γ–pretreated wells, IFN-γ was added post infection at the same concentration. For enumeration of CFU, infected BMDM were washed with PBS and lysed in water containing 0.1% Triton X-100 for 10 min. Serial dilutions were prepared in PBS with 0.05% Tween 80 and were plated onto 7H10 plates. Supernatant nitrite was measured by Griess assay as a proxy for NO production by mixing supernatant 1:1 with a solution of 0.1% napthylethylenediamine, 1% sulfanilamide, and 2% phosphoric acid and measuring absorbance at 546nm with a SpectraMax M2 microplate reader (Molecular Devices).

Immunofluorescent microscopy. Lung tissues were fixed in 10% neutral-buffered formalin at room temperature for 24 hours. Tissue embedding and sectioning at 5µM was performed by the

Center for Genomic Pathology Laboratory (UC Davis) and staining for anti-CD4 (D7D2Z, Cell Signaling Technology, Danvers, MA), anti-CD11b (M1/70, BioLegend) and anti-Ly6G (1A8, BioLegend) were performed by NanoString Technologies (Seattle, WA). Analysis of images for quantification was performed using ImageJ.

scRNA-seq and transcriptional analysis. The second largest lung lobes were pooled from five infected mice, tissue dissociated in RPMI 1640 containing liberase and DNase I in gentleMACS C tubes using the gentleMACS dissociator, strained through a 70 μM Falcon cell strainer in RPMI 1640 and counted. A total of 10,000 cells per sample were used for scRNAseq according to the 10x Genomics protocol. Briefly, single-cell suspensions were partitioned into Gel Beads in emulsion using the Chromium Next GEM Single Cell v3.1 system. Barcoded primers were used to reverse-transcribe poly-adenylated mRNA to produce barcoded, full-length cDNA. Purified DNA was amplified, fragmented, and amplified again to attach Illumina adapter sequences by the Functional Genomics Laboratory at UC, Berkeley. Libraries were sequenced on an Illumina NovaSeq S1 demultiplexed by the Vincent J. Coates Genomics Sequencing Laboratory at UC, Berkeley. Reads were aligned to the mouse transcriptome mm10 with the 10x Cell Ranger analysis pipeline using the Savio computational cluster at UC, Berkeley. After filtering, barcode counting, and unique molecular identifier counting, the Seurat 4.0.6 toolkit (Satija lab (Hao et al., 2021)) was used to preprocess the data. Dimension reduction (PCA) and κ-nearest neighbor graph construction (25 PCs) was followed by clustering (resolution 0.75) and visualization of the data with UMAP reduction. The clustered data were manually assigned a cell type using signature genes and gene expression and visualization was explored using Seurat (Table S1). GO terms were analyzed using the top 200 differentially expressed genes of each dataset. For neutrophil and macrophage/monocyte analysis, the relevant cells were subset, variable features were re-identified and the data rescaled within the subset. Dimension reduction (PCA) and κ-nearest neighbor graph construction (first 25 PCs), clustering (resolution 0.75) was followed by visualization and data exploration with the UMAP reduction. Differential gene expression was performed with Seurat's FindMarkers function. Gene ontology analysis was performed with topGO (v 2.48.0). The baseline of expression of neutrophil related genes in mouse immune cells types (Fig S4) was obtained from the Immunological Genome Project MyGeneset application (http://rstats.immgen.org/MyGeneSet_New/index.html) using the ImmGen ULI RNA-seq dataset.

Statistical analysis. Data are presented as mean values, and error bars represent SD. Symbols represent individual animals. The statistical tests used are denoted in the legend of the corresponding figure for each experiment. Analysis of statistical significance was performed using GraphPad Prism 8 (GraphPad, La Jolla, CA), and $p < 0.05$ was considered significant.

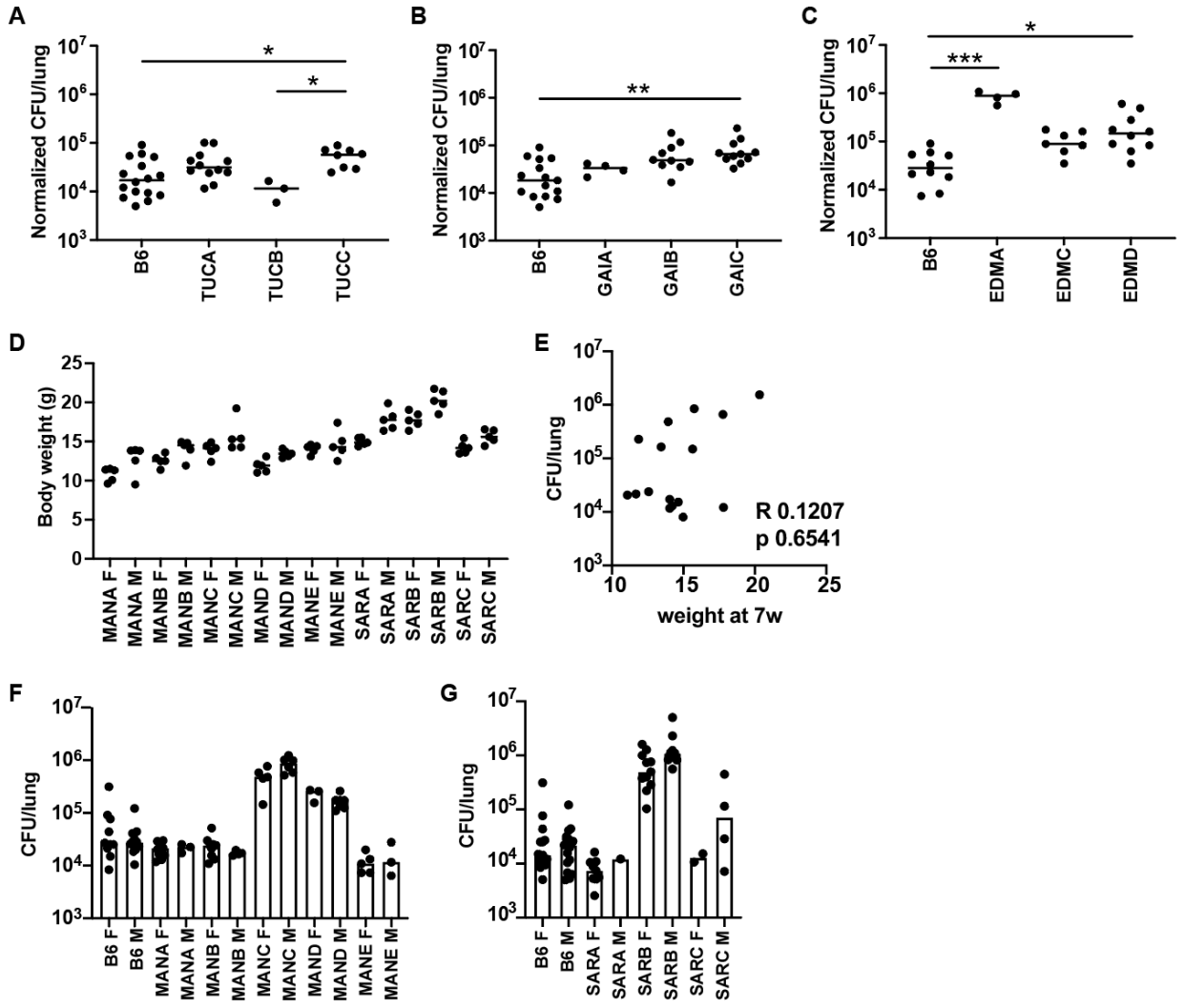

Figure S1. Variation in susceptibility to infection does not depend on mouse weight. CFU in the lungs of mice from (A) Tucson (B) Gainesville and (C) Edmonton at 21 days post infection were enumerated by CFU. (D) Body weight of adult male (M) and female (F) mice at age 7 weeks of age. (E) Spearman correlation analysis of CFU in the lungs vs weight at 7 weeks. (F,G) CFU data from the lungs of mice at 21d post infection broken down by both sex and genotype. CFU data was normalized to CFU enumeration on day 1 to correct for variation in inoculum dose between experimental days. Data represent 2-3 independent experiments, except for a single experiment for the TUCC, EDMA, EDMC and EDMD lines. Each dot represents a mouse. *p<0.05, **p<0.01, ***p<0.001 by Mann Whitney U test.

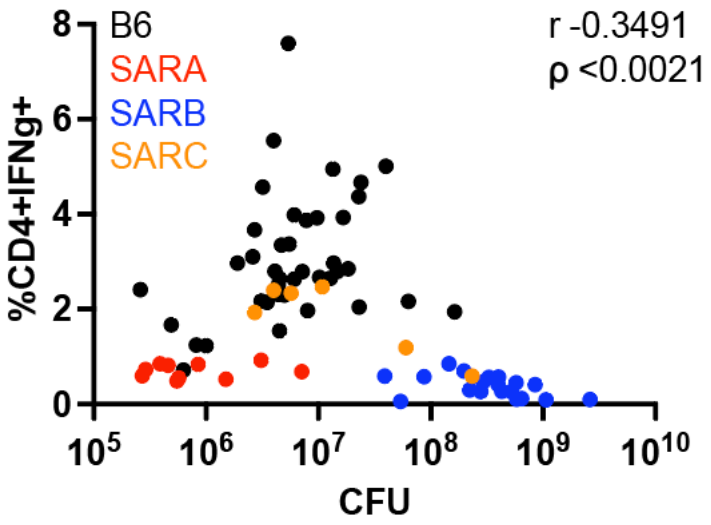

Figure S2. The proportion of IFN-γ producing CD4 T cells in the lung does not correlate with bacterial burden. Spearman correlation of CFU vs CD4+IFN-γ+ cells in the lungs of B6 or SARA, SARB and SARC mouse lines infected with *Mtb* enumerated at 21 days post infection. Data represent at least 2 independent experiments per line. The *p* value was determined using two-tailed Spearman correlations.

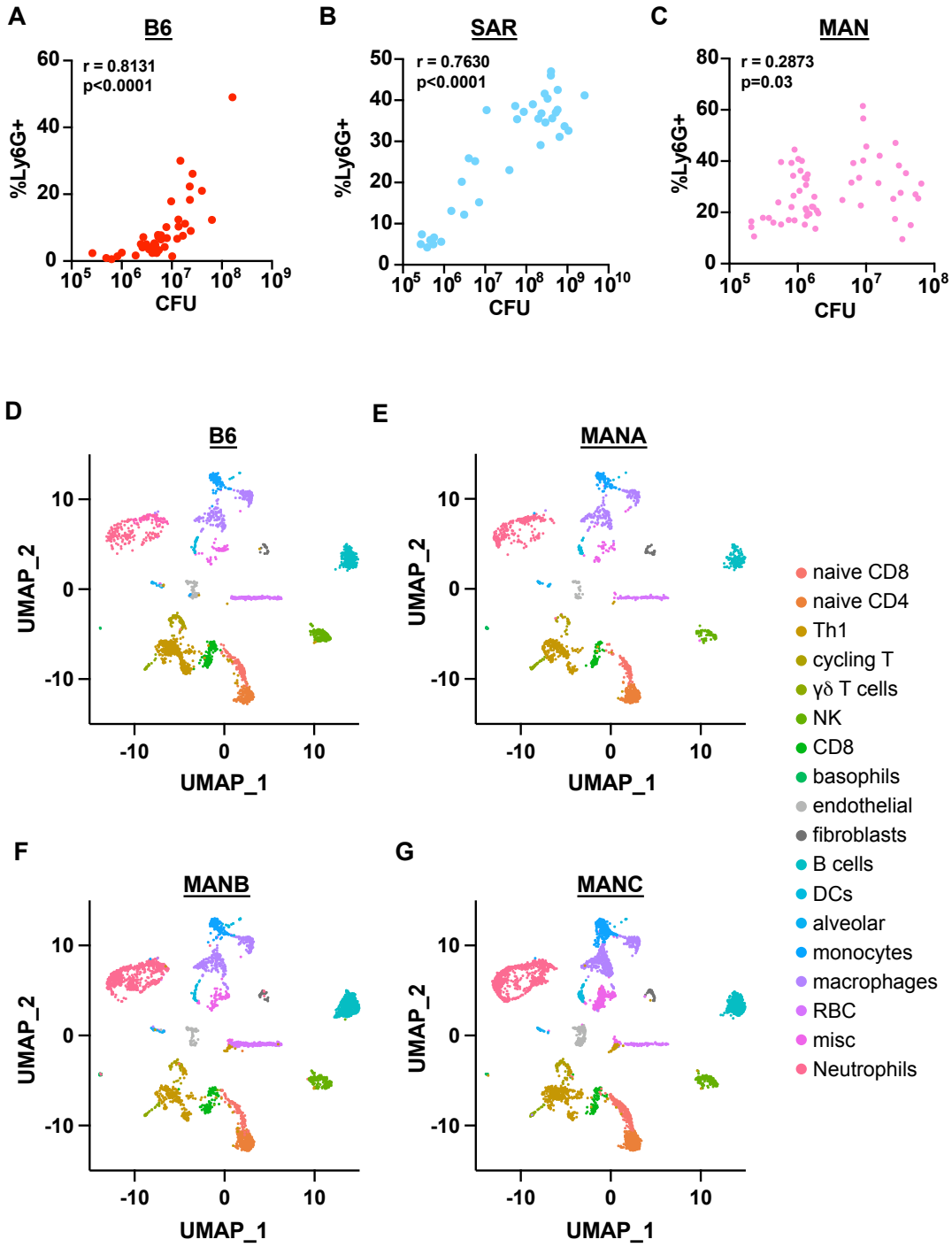

Figure S3. Immune cell composition in the lungs of infected mice. Spearman correlations between bacterial burden and presence of neutrophils (CD11b+Ly6G+) in the lung of infected B6 (A), Saratoga (B) and Manaus (C) mice. (D-G) UMAP plots of single cells isolated from the lungs of *Mtb* infected mice at 21 days post infection. (D) B6, (E) MANA, (F) MANB, (G) MANC.

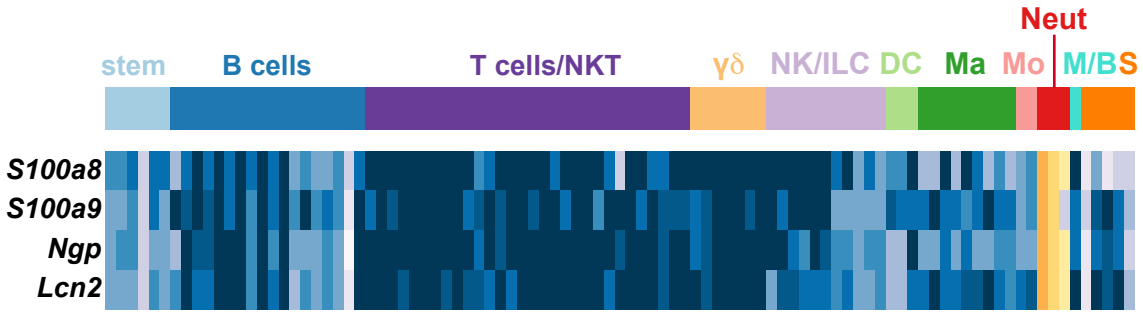

Figure S4. Gene expression across immune cells. Expression of indicated genes across immune cell types analyzed using Immunological Genome Project (ImmGen) MyGeneset application (http://rstats.immgen.org/MyGeneSet_New/index.html). Stem cells (stem); B cells; T cells/NK T cells (NKT); γδ T cells (γδ); Natural Killer/innate lymphoid cells (NK/ILC); dendritic cells (DC); macrophages (Ma); monocytes (Mo); neutrophils (Neut); Mast Cells/Basophils (M/B); Stromal Cells (S).

Table S1. Cellular expression markers used for scRNAseq cluster assignment following unbiased clustering.

Antonelli, L.R.V., A. Gigliotti Rothfuchs, R. Gonçalves, E. Roffê, A.W. Cheever, A. Bafica, A.M. Salazar, C.G. Feng, and A. Sher. 2010. Intranasal Poly-IC treatment exacerbates tuberculosis in mice through the pulmonary recruitment of a pathogen-permissive monocyte/macrophage population. *J. Clin. Invest.* 120:1674–1682. doi:10.1172/JCI40817.

Berry, M.P.R., C.M. Graham, F.W. McNab, Z. Xu, S.A.A. Bloch, T. Oni, K.A. Wilkinson, R. Banchereau, J. Skinner, R.J. Wilkinson, C. Quinn, D. Blankenship, R. Dhawan, J.J. Cush, A. Mejias, O. Ramilo, O.M. Kon, V. Pascual, J. Banchereau, D. Chaussabel, and A. O'Garra. 2010. An interferon-inducible neutrophil-driven blood transcriptional signature in human tuberculosis. *Nature*. 466:973–977. doi:10.1038/nature09247.

Bold, T.D., and J.D. Ernst. 2012. CD4+ T cell-dependent IFN-γ production by CD8+ effector T cells in Mycobacterium tuberculosis infection. *J. Immunol.* 189:2530–2536. doi:10.4049/jimmunol.1200994.

Cadena, A.M., J.L. Flynn, and S.M. Fortune. 2016. The Importance of First Impressions: Early Events in Mycobacterium tuberculosis Infection Influence Outcome. *MBio*. 7:e00342–16. doi:10.1128/mBio.00342-16.

Cadena, A.M., S.M. Fortune, and J.L. Flynn. 2017. Heterogeneity in tuberculosis. *Nat. Rev. Immunol.* 17:691–702. doi:10.1038/nri.2017.69.

Caruso, A.M., N. Serbina, E. Klein, K. Triebold, B.R. Bloom, and J.L. Flynn. 1999. Mice deficient in CD4 T cells have only transiently diminished levels of IFN-gamma, yet succumb to tuberculosis. *J. Immunol.* 162:5407–5416.

Churchill, G.A., D.C. Airey, H. Allayee, J.M. Angel, A.D. Attie, J. Beatty, W.D. Beavis, J.K. Belknap, B. Bennett, W. Berrettini, A. Bleich, M. Bogue, K.W. Broman, K.J. Buck, E. Buckler, M. Burmeister, E.J. Chesler, J.M. Cheverud, S. Clapcote, M.N. Cook, R.D. Cox, J.C. Crabbe, W.E. Crusio, A. Darvasi, C.F. Deschepper, R.W. Doerge, C.R. Farber, J. Forejt, D. Gaile, S.J. Garlow, H. Geiger, H. Gershenfeld, T. Gordon, J. Gu, W. Gu, G. de Haan, N.L. Hayes, C. Heller, H. Himmelbauer, R. Hitzemann, K. Hunter, H.-C. Hsu, F.A. Iraqi, B. Ivandic, H.J. Jacob, R.C. Jansen, K.J. Jepsen, D.K. Johnson, T.E. Johnson, G. Kempermann, C. Kendziorski, M. Kotb, R.F. Kooy, B. Llamas, F. Lammert, J.-M. Lassalle, P.R. Lowenstein, L. Lu, A. Lusis, K.F. Manly, R. Marcucio, D. Matthews, J.F. Medrano, D.R. Miller, G. Mittleman, B.A. Mock, J.S. Mogil, X. Montagutelli, G. Morahan, D.G. Morris, R. Mott, J.H. Nadeau, H. Nagase, R.S. Nowakowski, B.F. O'Hara, A.V. Osadchuk, G.P. Page, B. Paigen, K. Paigen, A.A. Palmer, H.-J. Pan, L. Peltonen-Palotie, J. Peirce, D. Pomp, M. Pravenec, D.R. Prows, Z. Qi, R.H. Reeves, J. Roder, G.D. Rosen, E.E. Schadt, L.C. Schalkwyk, Z. Seltzer, K. Shimomura, S. Shou, M.J. Sillanpää, L.D. Siracusa, H.-W. Snoeck, et al. 2004. The Collaborative Cross, a community resource for the genetic analysis of complex traits. *Nat. Genet.* 36:1133–1137. doi:10.1038/ng1104-1133.

Cohen, S.B., B.H. Gern, J.L. Delahaye, K.N. Adams, C.R. Plumlee, J.K. Winkler, D.R. Sherman, M.Y. Gerner, and K.B. Urdahl. 2018. Alveolar Macrophages Provide an Early Mycobacterium tuberculosis Niche and Initiate Dissemination. *Cell Host Microbe*. 24:439–446.e4. doi:10.1016/j.chom.2018.08.001.

Cooper, A.M., D.K. Dalton, T.A. Stewart, J.P. Griffin, D.G. Russell, and I.M. Orme. 1993. Disseminated tuberculosis in interferon gamma gene-disrupted mice. *J. Exp. Med.* 178:2243–2247. doi:10.1084/jem.178.6.2243.

Cyktor, J.C., B. Carruthers, P. Stromberg, E. Flaño, H. Pircher, and J. Turner. 2013. Killer cell lectin-like receptor G1 deficiency significantly enhances survival after Mycobacterium tuberculosis infection. *Infect. Immun.* 81:1090–1099. doi:10.1128/IAI.01199-12.

Desvignes, L., A.J. Wolf, and J.D. Ernst. 2012. Dynamic roles of type I and type II IFNs in early infection with Mycobacterium tuberculosis. *J. Immunol.* 188:6205–6215. doi:10.4049/jimmunol.1200255.

Dibbern, J., L. Eggers, and B.E. Schneider. 2017. Sex differences in the C57BL/6 model of Mycobacterium tuberculosis infection. *Sci. Rep.* 7:10957. doi:10.1038/s41598-017-11438-z.

Van Dis, E., D.M. Fox, H.M. Morrison, D.M. Fines, J.P. Babirye, L.H. McCann, S. Rawal, J.S. Cox, and S.A. Stanley. 2022. IFN-γ-independent control of M. tuberculosis requires CD4 T cell-derived GM-CSF and activation of HIF-1α. *PLoS Pathog.* 18:e1010721. doi:10.1371/journal.ppat.1010721.

Domingo-Gonzalez, R., O. Prince, A. Cooper, and S.A. Khader. 2016. Cytokines and Chemokines in Mycobacterium tuberculosis Infection. *Microbiol. Spectr.* 4. doi:10.1128/microbiolspec.TBTB2-0018-2016.

Donovan, M.L., T.E. Schultz, T.J. Duke, and A. Blumenthal. 2017. Type I interferons in the pathogenesis of tuberculosis: molecular drivers and immunological consequences. *Front. Immunol.* 8:1633. doi:10.3389/fimmu.2017.01633.

Dorhoi, A., C. Desel, V. Yeremeev, L. Pradl, V. Brinkmann, H.-J. Mollenkopf, K. Hanke, O. Gross, J. Ruland, and S.H.E. Kaufmann. 2010. The adaptor molecule CARD9 is essential for tuberculosis control. *J. Exp. Med.* 207:777–792. doi:10.1084/jem.20090067.

Dorhoi, A., V. Yeremeev, G. Nouailles, J. Weiner, S. Jörg, E. Heinemann, D. Oberbeck-Müller, J.K. Knaul, A. Vogelzang, S.T. Reece, K. Hahnke, H.-J. Mollenkopf, V. Brinkmann, and S.H.E. Kaufmann. 2014. Type I IFN signaling triggers immunopathology in tuberculosis-susceptible mice by modulating lung phagocyte dynamics. *Eur. J. Immunol.* 44:2380–2393. doi:10.1002/eji.201344219.

Eruslanov, E.B., I.V. Lyadova, T.K. Kondratieva, K.B. Majorov, I.V. Scheglov, M.O. Orlova, and A.S. Apt. 2005. Neutrophil responses to Mycobacterium tuberculosis infection in genetically susceptible and resistant mice. *Infect. Immun.* 73:1744–1753. doi:10.1128/IAI.73.3.1744-1753.2005.

Eum, S.-Y., J.-H. Kong, M.-S. Hong, Y.-J. Lee, J.-H. Kim, S.-H. Hwang, S.-N. Cho, L.E. Via, and C.E. Barry. 2010. Neutrophils are the predominant infected phagocytic cells in the airways of patients with active pulmonary TB. *Chest*. 137:122–128. doi:10.1378/chest.09-0903.

Ferris, K.G., A.S. Chavez, T.A. Suzuki, E.J. Beckman, M. Phifer-Rixey, K. Bi, and M.W. Nachman. 2021. The genomics of rapid climatic adaptation and parallel evolution in North American house mice. *PLoS Genet.* 17:e1009495. doi:10.1371/journal.pgen.1009495.

Flynn, J.L., J. Chan, K.J. Triebold, D.K. Dalton, T.A. Stewart, and B.R. Bloom. 1993. An essential role for interferon gamma in resistance to Mycobacterium tuberculosis infection. *J. Exp. Med.* 178:2249–2254. doi:10.1084/jem.178.6.2249.

Gallegos, A.M., J.W.J. van Heijst, M. Samstein, X. Su, E.G. Pamer, and M.S. Glickman. 2011. A gamma interferon independent mechanism of CD4 T cell mediated control of M. tuberculosis infection in vivo. *PLoS Pathog.* 7:e1002052. doi:10.1371/journal.ppat.1002052.

Gopal, R., L. Monin, D. Torres, S. Slight, S. Mehra, K.C. McKenna, B.A. Fallert Junecko, T.A. Reinhart, J. Kolls, R. Báez-Saldaña, A. Cruz-Lagunas, T.S. Rodríguez-Reyna, N.P. Kumar, P. Tessier, J. Roth, M. Selman, E. Becerril-Villanueva, J. Baquera-Heredia, B. Cumming, V.O. Kasprowicz, A.J.C. Steyn, S. Babu, D. Kaushal, J. Zúñiga, T. Vogl, J. Rangel-Moreno, and S.A. Khader. 2013. S100A8/A9 proteins mediate neutrophilic inflammation and lung pathology during tuberculosis. *Am. J. Respir. Crit. Care Med.* 188:1137–1146. doi:10.1164/rccm.201304-0803OC.

Green, A.M., R. Difazio, and J.L. Flynn. 2013. IFN-γ from CD4 T cells is essential for host survival and enhances CD8 T cell function during Mycobacterium tuberculosis infection. *J. Immunol.* 190:270–277. doi:10.4049/jimmunol.1200061.

Hao, Y., S. Hao, E. Andersen-Nissen, W.M. Mauck, S. Zheng, A. Butler, M.J. Lee, A.J. Wilk, C. Darby, M. Zager, P. Hoffman, M. Stoeckius, E. Papalexi, E.P. Mimitou, J. Jain, A. Srivastava, T. Stuart, L.M. Fleming, B. Yeung, A.J. Rogers, J.M. McElrath, C.A. Blish, R. Gottardo, P. Smibert, and R. Satija. 2021. Integrated analysis of multimodal single-cell data. *Cell*. 184:3573–3587.e29. doi:10.1016/j.cell.2021.04.048.

Heng, T.S.P., M.W. Painter, and Immunological Genome Project Consortium. 2008. The Immunological Genome Project: networks of gene expression in immune cells. *Nat. Immunol.* 9:1091–1094. doi:10.1038/ni1008-1091.

Ji, D.X., K.C. Witt, D.I. Kotov, S.R. Margolis, A. Louie, V. Chevée, K.J. Chen, M.M. Gaidt, H.S. Dhaliwal, A.Y. Lee, S.L. Nishimura, D.S. Zamboni, I. Kramnik, D.A. Portnoy, K.H. Darwin, and R.E. Vance. 2021. Role of the transcriptional regulator SP140 in resistance to bacterial infections via repression of type I interferons. *Elife*. 10. doi:10.7554/eLife.67290.

Ji, D.X., L.H. Yamashiro, K.J. Chen, N. Mukaida, I. Kramnik, K.H. Darwin, and R.E. Vance. 2019. Type I interferon-driven susceptibility to Mycobacterium tuberculosis is mediated by IL-1Ra. *Nat. Microbiol.* 4:2128–2135. doi:10.1038/s41564-019-0578-3.

Jiang, Z., P. Georgel, X. Du, L. Shamel, S. Sovath, S. Mudd, M. Huber, C. Kalis, S. Keck, C. Galanos, M. Freudenberg, and B. Beutler. 2005. CD14 is required for MyD88-independent LPS signaling. *Nat. Immunol.* 6:565–570. doi:10.1038/ni1207.

Keller, C., R. Hoffmann, R. Lang, S. Brandau, C. Hermann, and S. Ehlers. 2006. Genetically determined susceptibility to tuberculosis in mice causally involves accelerated and enhanced recruitment of granulocytes. *Infect. Immun.* 74:4295–4309. doi:10.1128/IAI.00057-06.

Kimmey, J.M., J.P. Huynh, L.A. Weiss, S. Park, A. Kambal, J. Debnath, H.W. Virgin, and C.L. Stallings. 2015. Unique role for ATG5 in neutrophil-mediated immunopathology during M. tuberculosis infection. *Nature*. 528:565–569. doi:10.1038/nature16451.

Koyuncu, D., M.K.K. Niazi, T. Tavolara, C. Abeijon, M. Ginese, Y. Liao, C. Mark, A.C. Gower, D.M. Gatti, I. Kramnik, M. Gurcan, B. Yener, and G. Beamer. 2021. Tuberculosis biomarkers discovered using Diversity Outbred mice. *medRxiv*. doi:10.1101/2021.01.08.20249024.

Kramnik, I., P. Demant, and B.B. Bloom. 1998. Susceptibility to tuberculosis as a complex genetic trait: analysis using recombinant congenic strains of mice. *Novartis Found Symp*. 217:120–31; discussion 132.

Kramnik, I., W.F. Dietrich, P. Demant, and B.R. Bloom. 2000. Genetic control of resistance to experimental infection with virulent Mycobacterium tuberculosis. *Proc. Natl. Acad. Sci. USA*. 97:8560–8565. doi:10.1073/pnas.150227197.

Leal, I.S., B. Smedegård, P. Andersen, and R. Appelberg. 2001. Failure to induce enhanced protection against tuberculosis by increasing T-cell-dependent interferon-gamma generation. *Immunology*. 104:157–161. doi:10.1046/j.1365-2567.2001.01305.x.

Lindenstrøm, T., N.P.H. Knudsen, E.M. Agger, and P. Andersen. 2013. Control of chronic mycobacterium tuberculosis infection by CD4 KLRG1- IL-2-secreting central memory cells. *J. Immunol.* 190:6311–6319. doi:10.4049/jimmunol.1300248.

Llibre, A., N. Bilek, V. Bondet, F. Darboe, S.K. Mbandi, A. Penn-Nicholson, M. Hatherill, F. Rozenberg, T.J. Scriba, and D. Duffy. 2019. Plasma type I IFN protein concentrations in human tuberculosis. *Front. Cell Infect. Microbiol.* 9:296. doi:10.3389/fcimb.2019.00296.

Lönnroth, K., B.G. Williams, P. Cegielski, and C. Dye. 2010. A consistent log-linear relationship between tuberculosis incidence and body mass index. *Int. J. Epidemiol.* 39:149–155. doi:10.1093/ije/dyp308.

Lowe, D.M., P.S. Redford, R.J. Wilkinson, A. O'Garra, and A.R. Martineau. 2012. Neutrophils in tuberculosis: friend or foe? *Trends Immunol.* 33:14–25. doi:10.1016/j.it.2011.10.003.

Lyadova, I.V., E.N. Tsiganov, M.A. Kapina, G.S. Shepelkova, V.V. Sosunov, T.V. Radaeva, K.B. Majorov, N.S. Shmitova, H.-J. van den Ham, V.V. Ganusov, R.J. De Boer, R. Racine, and G.M. Winslow. 2010. In mice, tuberculosis progression is associated with intensive inflammatory response and the accumulation of Gr-1 cells in the lungs. *PLoS One*. 5:e10469. doi:10.1371/journal.pone.0010469.

Majlessi, L., M. Simsova, Z. Jarvis, P. Brodin, M.-J. Rojas, C. Bauche, C. Nouzé, D. Ladant, S.T. Cole, P. Sebo, and C. Leclerc. 2006. An increase in antimycobacterial Th1-cell responses by prime-boost protocols of immunization does not enhance protection against tuberculosis. *Infect. Immun.* 74:2128–2137. doi:10.1128/IAI.74.4.2128-2137.2006.

Marzo, E., C. Vilaplana, G. Tapia, J. Diaz, V. Garcia, and P.-J. Cardona. 2014. Damaging role of neutrophilic infiltration in a mouse model of progressive tuberculosis. *Tuberculosis (Edinb)*. 94:55–64. doi:10.1016/j.tube.2013.09.004.

Mishra, B.B., R.R. Lovewell, A.J. Olive, G. Zhang, W. Wang, E. Eugenin, C.M. Smith, J.Y. Phuah, J.E. Long, M.L. Dubuke, S.G. Palace, J.D. Goguen, R.E. Baker, S. Nambi, R. Mishra, M.G. Booty, C.E. Baer, S.A. Shaffer, V. Dartois, B.A. McCormick, X. Chen, and C.M. Sassetti. 2017. Nitric oxide prevents a pathogen-permissive granulocytic inflammation during tuberculosis. *Nat. Microbiol.* 2:17072. doi:10.1038/nmicrobiol.2017.72.

Mittrücker, H.-W., U. Steinhoff, A. Köhler, M. Krause, D. Lazar, P. Mex, D. Miekley, and S.H.E. Kaufmann. 2007. Poor correlation between BCG vaccination-induced T cell responses and protection against tuberculosis. *Proc. Natl. Acad. Sci. USA*. 104:12434–12439. doi:10.1073/pnas.0703510104.

Moeller, A.H., T.A. Suzuki, M. Phifer-Rixey, and M.W. Nachman. 2018. Transmission modes of the mammalian gut microbiota. *Science*. 362:453–457. doi:10.1126/science.aat7164.

Mogues, T., M.E. Goodrich, L. Ryan, R. LaCourse, and R.J. North. 2001. The relative importance of T cell subsets in immunity and immunopathology of airborne Mycobacterium tuberculosis infection in mice. *J. Exp. Med.* 193:271–280. doi:10.1084/jem.193.3.271.

Moreira-Teixeira, L., P.J. Stimpson, E. Stavropoulos, S. Hadebe, P. Chakravarty, M. Ioannou, I.V. Aramburu, E. Herbert, S.L. Priestnall, A. Suarez-Bonnet, J. Sousa, K.L. Fonseca, Q. Wang, S. Vashakidze, P. Rodríguez-Martínez, C. Vilaplana, M. Saraiva, V. Papayannopoulos, and A. O'Garra. 2020a. Type I IFN exacerbates disease in tuberculosis-susceptible mice by inducing neutrophil-mediated lung inflammation and NETosis. *Nat. Commun.* 11:5566. doi:10.1038/s41467-020-19412-6.

Moreira-Teixeira, L., O. Tabone, C.M. Graham, A. Singhania, E. Stavropoulos, P.S. Redford, P. Chakravarty, S.L. Priestnall, A. Suarez-Bonnet, E. Herbert, K.D. Mayer-Barber, A. Sher, K.L. Fonseca, J. Sousa, B. Cá, R. Verma, P. Haldar, M. Saraiva, and A. O'Garra. 2020b. Mouse transcriptome reveals potential signatures of protection and pathogenesis in human tuberculosis. *Nat. Immunol.* 21:464–476. doi:10.1038/s41590-020-0610-z.

Nair, S., J.P. Huynh, V. Lampropoulou, E. Loginicheva, E. Esaulova, A.P. Gounder, A.C.M. Boon, E.A. Schwarzkopf, T.R. Bradstreet, B.T. Edelson, M.N. Artyomov, C.L. Stallings, and M.S. Diamond. 2018. Irg1 expression in myeloid cells prevents immunopathology during M. tuberculosis infection. *J. Exp. Med.* 215:1035–1045. doi:10.1084/jem.20180118.

Nandi, B., and S.M. Behar. 2011. Regulation of neutrophils by interferon-γ limits lung inflammation during tuberculosis infection. *J. Exp. Med.* 208:2251–2262. doi:10.1084/jem.20110919.

Niazi, M.K.K., N. Dhulekar, D. Schmidt, S. Major, R. Cooper, C. Abeijon, D.M. Gatti, I. Kramnik, B. Yener, M. Gurcan, and G. Beamer. 2015. Lung necrosis and neutrophils reflect

common pathways of susceptibility to Mycobacterium tuberculosis in genetically diverse, immune-competent mice. *Dis. Model. Mech.* 8:1141–1153. doi:10.1242/dmm.020867.

Nogueira, B.M.F., S. Krishnan, B. Barreto-Duarte, M. Araújo-Pereira, A.T.L. Queiroz, J.J. Ellner, P. Salgame, T.J. Scriba, T.R. Sterling, A. Gupta, and B.B. Andrade. 2022. Diagnostic biomarkers for active tuberculosis: progress and challenges. *EMBO Mol. Med.* 14:e14088. doi:10.15252/emmm.202114088.

Pan, H., B.-S. Yan, M. Rojas, Y.V. Shebzukhov, H. Zhou, L. Kobzik, D.E. Higgins, M.J. Daly, B.R. Bloom, and I. Kramnik. 2005. Ipr1 gene mediates innate immunity to tuberculosis. *Nature*. 434:767–772. doi:10.1038/nature03419.

Phifer-Rixey, M., K. Bi, K.G. Ferris, M.J. Sheehan, D. Lin, K.L. Mack, S.M. Keeble, T.A. Suzuki, J.M. Good, and M.W. Nachman. 2018. The genomic basis of environmental adaptation in house mice. *PLoS Genet.* 14:e1007672. doi:10.1371/journal.pgen.1007672.

Qu, H.-Q., Q. Li, J.B. McCormick, and S.P. Fisher-Hoch. 2011. What did we learn from the genome-wide association study for tuberculosis susceptibility? *J. Med. Genet.* 48:217–218. doi:10.1136/jmg.2010.087361.

Ravesloot-Chávez, M.M., E. Van Dis, and S.A. Stanley. 2021. The Innate Immune Response to Mycobacterium tuberculosis Infection. *Annu. Rev. Immunol.* 39:611–637. doi:10.1146/annurev-immunol-093019-010426.

Rothchild, A.C., P. Jayaraman, C. Nunes-Alves, and S.M. Behar. 2014. iNKT cell production of GM-CSF controls Mycobacterium tuberculosis. *PLoS Pathog.* 10:e1003805. doi:10.1371/journal.ppat.1003805.

Rothchild, A.C., B. Stowell, G. Goyal, C. Nunes-Alves, Q. Yang, K. Papavinasasundaram, C.M. Sassetti, G. Dranoff, X. Chen, J. Lee, and S.M. Behar. 2017. Role of Granulocyte-Macrophage Colony-Stimulating Factor Production by T Cells during Mycobacterium tuberculosis Infection. *MBio*. 8. doi:10.1128/mBio.01514-17.

Sakai, S., K.D. Kauffman, M.A. Sallin, A.H. Sharpe, H.A. Young, V.V. Ganusov, and D.L. Barber. 2016. CD4 T Cell-Derived IFN-γ Plays a Minimal Role in Control of Pulmonary Mycobacterium tuberculosis Infection and Must Be Actively Repressed by PD-1 to Prevent Lethal Disease. *PLoS Pathog.* 12:e1005667. doi:10.1371/journal.ppat.1005667.

Sakai, S., K.D. Kauffman, J.M. Schenkel, C.C. McBerry, K.D. Mayer-Barber, D. Masopust, and D.L. Barber. 2014. Cutting edge: control of Mycobacterium tuberculosis infection by a subset of lung parenchyma-homing CD4 T cells. *J. Immunol.* 192:2965–2969. doi:10.4049/jimmunol.1400019.

Salcedo, T., A. Geraldes, and M.W. Nachman. 2007. Nucleotide variation in wild and inbred mice. *Genetics*. 177:2277–2291. doi:10.1534/genetics.107.079988.

Scanga, C.A., V.P. Mohan, K. Yu, H. Joseph, K. Tanaka, J. Chan, and J.L. Flynn. 2000. Depletion of CD4(+) T cells causes reactivation of murine persistent tuberculosis despite continued expression of interferon gamma and nitric oxide synthase 2. *J. Exp. Med.* 192:347–358. doi:10.1084/jem.192.3.347.

Scriba, T.J., A. Penn-Nicholson, S. Shankar, T. Hraha, E.G. Thompson, D. Sterling, E. Nemes, F. Darboe, S. Suliman, L.M. Amon, H. Mahomed, M. Erasmus, W. Whatney, J.L. Johnson, W.H. Boom, M. Hatherill, J. Valvo, M.A. De Groote, U.A. Ochsner, A. Aderem, W.A. Hanekom, D.E. Zak, and other members of the ACS cohort study team. 2017. Sequential inflammatory processes define human progression from M. tuberculosis infection to tuberculosis disease. *PLoS Pathog.* 13:e1006687. doi:10.1371/journal.ppat.1006687.

Singhania, A., R. Verma, C.M. Graham, J. Lee, T. Tran, M. Richardson, P. Lecine, P. Leissner, M.P.R. Berry, R.J. Wilkinson, K. Kaiser, M. Rodrigue, G. Woltmann, P. Haldar, and A. O'Garra. 2018. A modular transcriptional signature identifies phenotypic heterogeneity of human tuberculosis infection. *Nat. Commun.* 9:2308. doi:10.1038/s41467-018-04579-w.

Smith, C.M., R.E. Baker, M.K. Proulx, B.B. Mishra, J.E. Long, S.W. Park, H.-N. Lee, M.C. Kiritsy, M.M. Bellerose, A.J. Olive, K.C. Murphy, K. Papavinasasundaram, F.J. Boehm, C.J. Reames, R.K. Meade, B.K. Hampton, C.L. Linnertz, G.D. Shaw, P. Hock, T.A. Bell, S. Ehrt, D. Schnappinger, F. Pardo-Manuel de Villena, M.T. Ferris, T.R. Ioerger, and C.M. Sassetti. 2022. Host-pathogen genetic interactions underlie tuberculosis susceptibility in genetically diverse mice. *Elife*. 11. doi:10.7554/eLife.74419.

Smith, C.M., M.K. Proulx, R. Lai, M.C. Kiritsy, T.A. Bell, P. Hock, F. Pardo-Manuel de Villena, M.T. Ferris, R.E. Baker, S.M. Behar, and C.M. Sassetti. 2019. Functionally overlapping variants control tuberculosis susceptibility in collaborative cross mice. *MBio*. 10. doi:10.1128/mBio.02791-19.

Smith, C.M., M.K. Proulx, A.J. Olive, D. Laddy, B.B. Mishra, C. Moss, N.M. Gutierrez, M.M. Bellerose, P. Barreira-Silva, J.Y. Phuah, R.E. Baker, S.M. Behar, H. Kornfeld, T.G. Evans, G. Beamer, and C.M. Sassetti. 2016. Tuberculosis susceptibility and vaccine protection are independently controlled by host genotype. *MBio*. 7. doi:10.1128/mBio.01516-16.

Srivastava, S., J.D. Ernst, and L. Desvignes. 2014. Beyond macrophages: the diversity of mononuclear cells in tuberculosis. *Immunol. Rev.* 262:179–192. doi:10.1111/imr.12217.

Stanley, S.A., J.E. Johndrow, P. Manzanillo, and J.S. Cox. 2007. The Type I IFN response to infection with Mycobacterium tuberculosis requires ESX-1-mediated secretion and contributes to pathogenesis. *J. Immunol.* 178:3143–3152. doi:10.4049/jimmunol.178.5.3143.

Suzuki, T.A., F.M. Martins, M. Phifer-Rixey, and M.W. Nachman. 2020. The gut microbiota and Bergmann's rule in wild house mice. *Mol. Ecol.* 29:2300–2311. doi:10.1111/mec.15476.

Svenson, K.L., D.M. Gatti, W. Valdar, C.E. Welsh, R. Cheng, E.J. Chesler, A.A. Palmer, L. McMillan, and G.A. Churchill. 2012. High-resolution genetic mapping using the Mouse Diversity Outbred population. *Genetics*. 190:437–447. doi:10.1534/genetics.111.132597.

Tait, D.R., M. Hatherill, O. Van Der Meeren, A.M. Ginsberg, E. Van Brakel, B. Salaun, T.J. Scriba, E.J. Akite, H.M. Ayles, A. Bollaerts, M.-A. Demoitié, A. Diacon, T.G. Evans, P. Gillard, E. Hellström, J.C. Innes, M. Lempicki, M. Malahleha, N. Martinson, D. Mesia Vela, M. Muyoyeta, V. Nduba, T.G. Pascal, M. Tameris, F. Thienemann, R.J. Wilkinson, and F. Roman. 2019. Final analysis of a trial of M72/AS01E vaccine to prevent tuberculosis. *N. Engl. J. Med.* 381:2429–2439. doi:10.1056/NEJMoa1909953.

Tameris, M.D., M. Hatherill, B.S. Landry, T.J. Scriba, M.A. Snowden, S. Lockhart, J.E. Shea, J.B. McClain, G.D. Hussey, W.A. Hanekom, H. Mahomed, H. McShane, and MVA85A 020 Trial Study Team. 2013. Safety and efficacy of MVA85A, a new tuberculosis vaccine, in infants previously vaccinated with BCG: a randomised, placebo-controlled phase 2b trial. *Lancet*. 381:1021–1028. doi:10.1016/S0140-6736(13)60177-4.

Yang, H., J.R. Wang, J.P. Didion, R.J. Buus, T.A. Bell, C.E. Welsh, F. Bonhomme, A.H.-T. Yu, M.W. Nachman, J. Pialek, P. Tucker, P. Boursot, L. McMillan, G.A. Churchill, and F.P.-M. de Villena. 2011. Subspecific origin and haplotype diversity in the laboratory mouse. *Nat. Genet.* 43:648–655. doi:10.1038/ng.847.

Zak, D.E., A. Penn-Nicholson, T.J. Scriba, E. Thompson, S. Suliman, L.M. Amon, H. Mahomed, M. Erasmus, W. Whatney, G.D. Hussey, D. Abrahams, F. Kafaar, T. Hawkridge, S. Verver, E.J. Hughes, M. Ota, J. Sutherland, R. Howe, H.M. Dockrell, W.H. Boom, B. Thiel, T.H.M. Ottenhoff, H. Mayanja-Kizza, A.C. Crampin, K. Downing, M. Hatherill, J. Valvo, S. Shankar, S.K. Parida, S.H.E. Kaufmann, G. Walzl, A. Aderem, W.A. Hanekom, and ACS and GC6-74 cohort study groups. 2016. A blood RNA signature for tuberculosis disease risk: a prospective cohort study. *Lancet*. 387:2312–2322. doi:10.1016/S0140-6736(15)01316-1.